

# NSLS-II Project

## **CONCEPTUAL DESIGN REPORT for the COHERENT HARD X-RAY BEAMLINE AT NSLS-II**



final draft Sep 2009

*Intentionally blank.*

## Approvals and Reviewers

### Compiled by

Andrei Fluerasu, CHX Beamline Scientist, NSLS-II

### Approved

Qun Shen, XFD Director, NSLS-II

### Reviewers

Robert L. Leheny, BAT Spokesperson, on behalf of the BAT

Andy Broadbent, Beamlines Manager

Nicholas Gmür, ESH Coordinator, NSLS-II

Sushil Sharma, Mechanical Engineering Group Leader, NSLS-II

### Signature

### Date

## Document Updates

The Conceptual Design Report for the Coherent Hard X-ray Beamline at NSLS-II is a controlled document, revised under change control.

Version No.	Date	Changes made
A	5/13/2009	Initial draft, submitted to BAT
B	9/16/2009	Second submittal to BAT, and first to editing
1	10/1/2009	Final draft, submitted to BAT

*Intentionally blank.*

## Contents

1	INTRODUCTION .....	1
1.1	Scientific Requirements .....	1
	Glassy Dynamics in Soft Matter .....	2
	Phase Behavior and Dynamics on Liquid and Solid Surfaces .....	3
	Coherent Diffraction Imaging .....	3
	New Investigation Methods; Instrumental Developments .....	3
1.2	Coherent Hard X-ray Beamline Team .....	3
	Beamline Scientists .....	3
	NSLS-II Management and Engineering Support .....	4
	Beamline Advisory Team (BAT) .....	4
2	BEAMLINE LAYOUT .....	5
2.1	Overview .....	5
2.2	Insertion Device .....	9
2.3	Front End .....	11
2.4	Optical Layout .....	13
	White Beam Mirror .....	13
	Secondary Slits .....	14
	Be CRLs for Vertical Focusing .....	14
	Monochromator(s) .....	14
2.5	High Heat Load Optics .....	17
2.6	Beamline Optics and Coherence Preservation .....	17
2.7	Ray Tracing .....	18
2.8	List of Major Components .....	18
2.9	End Station Instrumentation .....	19
3	SPECIAL BEAMLINE REQUIREMENTS .....	21
3.1	Vacuum .....	21
3.2	Detectors .....	21
3.3	Synchrotron Filling Modes .....	22
3.4	Data Storage/Handling .....	22
4	FUTURE UPGRADE OPTIONS .....	23
4.1	Detector Developments .....	23
4.2	Specialized Sample Environments .....	23
4.3	Beamline Optics and Figure Control .....	23
APPENDIX 1	SCHEDULE .....	25
APPENDIX 2	REFERENCE DRAWINGS .....	27

## Acronyms

ADP	Avalanche Photon Diode
Be	Beryllium
CDI	Coherent Diffraction Imaging
CRL	Compound Refractive Lens
DCM	Double Crystal Monochromator
DW	Damping Wiggler
EH	Experimental Hutch
FEA	Finite Element Analysis
GI-SAXS	Grazing Incidence Small Angle X-ray Scattering
LOI	Letter of Intent
ML	Multi Layers
OH	Optics Hutch
SAXS	Small Angle X-ray Scattering
SNR	Signal-to-Noise Ratio
SVS	Speckle Visibility Spectroscopy
UHV	Ultra High Vacuum
VIPIC	Vertically Integrating Pixel Imaging Chip
WAXS	Wide Angle X-ray Scattering
XPCS	X-ray Photon Correlation Spectroscopy

# 1 INTRODUCTION

## 1.1 Scientific Requirements

The Coherent Hard X-ray (CHX) beamline at NSLS-II will be dedicated to studies of nanometer-scale dynamics in materials using X-ray Photon Correlation Spectroscopy (XPCS), and to other experimental methods enabled by bright, coherent, X-ray beams. XPCS is based on measuring time correlation functions of the speckle fluctuations that occur when a coherent X-ray beam is scattered from a disordered sample. It can be used to measure equilibrium dynamics via the “usual” single-speckle intensity-intensity autocorrelation functions  $g^{(2)}(q, t)$ . If combined with 2D area detectors and a multispeckle technique, it can also be used to measure non-stationary, non-equilibrium dynamics via two-time correlation functions  $g^{(2)}(q, t_1, t_2)$ . Higher order correlation functions  $g^{(n)}(q, t)$  can be used to characterize heterogeneities in the dynamical properties.

The key quantity that enables XPCS experiments is the source brightness. This determines the flux of coherent X-ray photons and ultimately the signal-to-noise ratio (SNR) of the measured correlation functions. The technique was first demonstrated in pioneering experiments that become possible at NSLS (M. Sutton et al., *Nature* **352**, 608, 1991; S. Dierker et al., *Phys. Rev. Lett.* **75**, 449, 1995) and later “moved” to brighter 3<sup>rd</sup> generation Synchrotron sources such as ESRF and APS. With the unprecedented brilliance of the NSLS-II storage ring exceeding  $10^{21}$  photons/s/mrad<sup>2</sup>/mm<sup>2</sup>/0.1 % bw for a photon energy near E~8 keV (more than one order of magnitude higher than that of the Advanced Photon Source), the CHX beamline will allow studies of dynamics on time scales that can be  $\sim 10^2=100$  times faster and on shorter length scales than was ever possible before (Figure 1). The experiments will be performed in a variety of scattering geometries such as small angle scattering (SAXS), wide angle scattering (WAXS) or grazing incidence small angle scattering (GI-SAXS) and the proposed instrument will provide the required flexibility to efficiently adapt to all these situations. The design of the CHX instrument is simple and robust and puts an emphasis on three key elements:

- coherence (brilliance) preservation by carefully designing and engineering key optical elements, reducing the number of windows, mirrors, etc. to an absolute minimum
- maximizing the useful signal by using the entire available coherent flux (via focusing optics)
- maximizing the mechanical stability of the instrument

With specific sample environments which will be hosted on a versatile diffractometer, and a slightly different alignment/tuning, the CHX instrument will also be ideally suited for Coherent Diffraction Imaging (CDI) and micro-beam solution small-angle scattering. Developing these techniques, especially for studies of biological systems, is an important part of the scientific program of the beamline.

There are several classes of XPCS experiments that will probe a combination of length- and time-scales that are fundamentally important, and which are very difficult or impossible to measure at other (less bright) facilities or by using other techniques. These include, but are not limited to:

- Glassy materials, driven and out-of-equilibrium systems
- Colloids, polymers, and nanostructured complex fluids
- Biological systems such as proteins in solution and biomembranes
- Dynamics at fluid surfaces and interfaces
- molecular dynamics and metallic and orientational glasses; dynamics at solid surfaces
- $\mu$ -beam SAXS studies on the kinetics of biological processes: protein and RNA folding, protein crystallization and explorations of solvent conditions
- X-ray microscopy via coherent diffraction imaging on biological systems as close as possible to their native state (frozen, hydrated)

The scientific program which will be pursued through active collaborations between the user community and the CHX group is described in detail in the XPCS LOI document, “A Coherent Hard X-ray Beamline for XPCS and Microbeam SAXS at NSLS-II” and will not be included here in its integrality. A subset of the proposed area of research, which will likely lie at the core of the in-house research program in the CHX group is briefly described below. These “in-house” studies will require instrumental developments, new sample environments, etc. and will undoubtedly become available and useful to the extended user community. Ultimately, such an approach enables new applications and results that otherwise would not be within reach.

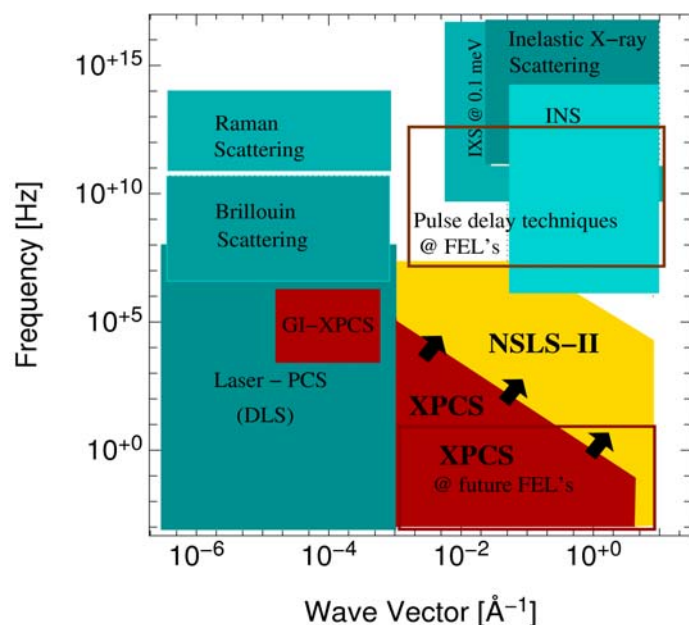


**Figure 1** Wave vector – frequency phase-space currently occupied by XPCS at 3<sup>rd</sup> generation light sources. The goal of the CHX beamline at NSLS-II is to extend this region toward faster time scales and shorter length scales (gold). With its unprecedented brilliance, NSLS-II result could approach (if not match) the faster time scales accessible with neutron spin-echo and close the gap that currently exists in the phase space. This dynamic range will also fall in the gap left open by the future FELs between “classic” XPCS experiments using the high average brilliance of these sources, but being limited by their pulsed structure, and pulse delay techniques being limited by practical considerations such as the size of delay lines. This will make NSLS-II a truly unique instrument for XPCS.

### Glassy Dynamics in Soft Matter

Understanding the underlying mechanism by which model systems such as highly interactive colloidal suspensions arrest to non-equilibrium states and form glasses and/or gels is a fundamental problem in condensed matter physics. As the system approaches the glass transition, the dynamics start slowing down without an obvious reason in the structural (static) properties of the system. At the same time different relaxation modes become increasingly separated in time - e.g. fast modes associated with the motion of individual constituents hindered by neighboring particles and slow modes associated with the motion of groups (cages) of particles. Understanding the glass (or gel) transition is a problem of tremendous fundamental interest in soft matter physics. Solving it will also help us in better understanding phenomena like protein aggregation, which are responsible, for instance, for the cataract formation in the human eye lens or for the neuronal cell death associated with Alzheimer's disease. With their relatively slow dynamical relaxation modes occurring on molecular length scales, glassy systems are well suited for XPCS and very recent results obtained at existing 3<sup>rd</sup> generation light sources (mainly ID10, ESRF and 8ID, APS) have provided an invaluable insight into the mechanisms associated with the slow relaxation modes. At NSLS-II it will become possible to extend the dynamic range by several decades, hence measure also the fast relaxation modes. The tremendous increase in brilliance and special sample handling techniques (e.g., using microfluidic techniques to avoid beam damage and achieve new functionalities – A. Fluerasu et al., *J. Synch. Rad.* **15**, 378, 2008) may also enable, for the first time, studies of dynamics in biological systems such as protein aggregation in a solution.

A second key advantage for the study of glassy dynamics at NSLS-II will be associated with the study of dynamical spatial or temporal heterogeneities. With the high brilliance source, it will be possible to achieve smaller beam sizes to probe smaller volumes or to go beyond analyzing the intensity fluctuations via the second order correlation functions  $g^{(2)}(q, t)$  and measure “fluctuations of intensity fluctuations” via higher order correlation functions  $g^{(n)}(q, t)$ . Such studies have been limited thus far, mainly because the even more stringent requirements they put on the source, i.e. the signal-to-noise ratio (SNR). The SNR is proportional with the square of the source brilliance  $B^2$  for 4<sup>th</sup> order correlation functions  $g^{(4)}(q, t)$ , while only proportional to  $B$  in  $g^{(2)}(q, t)$ .



### Phase Behavior and Dynamics on Liquid and Solid Surfaces

The structure, phase behavior and dynamical properties of liquid and solid interfaces can be studied using a grazing-incidence scattering geometry. Current research includes biological films at liquid-vapor interfaces, bio-membranes, etc. The CHX beamline will enable studies on faster time scales than possible today and will facilitate studies of the interplay between surface induced order and surface dynamics in systems such as alkanes undergoing surface freezing.

### Coherent Diffraction Imaging

Imaging of biological systems such as a whole cell in their native state (unstained, unsectioned, etc.) in three dimensions is of a fundamental importance in cellular biology, and hard X-ray coherent diffraction imaging is arguably the best experimental tool that can achieve this task, given the high penetration depths, and the fine resolution that can be obtained (E. Lima, L. Wiegart et al., accepted *Phys. Rev. Lett.*, 2009). Since the CHX instrument will be optimized to reduce to an absolute minimum any distortions to the coherent wave front, it will offer an ideal instrument for CDI experiments in the forward (SAXS) direction.

### New Investigation Methods; Instrumental Developments

The continuous optimization of the CHX instrument by pushing the signal-to-noise level for XPCS and/or CDI experiments to a maximum is, and will remain, a central activity in the CHX group. At the same time, a vigorous research program aiming at developing new investigation tools will hopefully help “pushing the boundaries” of the phase space shown in Figure 1. An example of such a development is that of X-ray Speckle Visibility Spectroscopy (XSVS). This method allows the direct measurement of nanometer-scale dynamics in materials by analyzing a single “speckle pattern”. The main idea, which follows the development of *speckle visibility spectroscopy* recently proposed for visible light (P.K. Dixon and D.J. Durian, *Phys. Rev. Lett.* **90**, 184302, 2003), is that the speckle contrast depends on the characteristic time scales of fluctuations in the sample, hence it is possible to resolve the dynamics over a wide range of length scales by analyzing the speckle visibility across a *single* diffraction pattern obtained with a 2D area detector. XSVS will be ideally suited to study dynamics at the high brilliance CHX beamline. As XSVS does not require a continuous time series but only single speckle patterns (with the acquisition time determined by the software trigger of the detector or by a fast shutter), it will offer the possibility to access shorter time scales, beyond the corresponding maximum frame rate of the detector. Since it only requires single images – i.e. “snapshots” – it will offer a unique way of measuring the “instantaneous” dynamics in complex systems with heterogeneous and/or intermittent behavior. In addition, it will also help avoiding beam damage in many soft matter or biological systems as the total required dose will be significantly reduced. Finally, XSVS may allow adopting a “flash approach” in measuring, for instance, the dynamics in a protein crystal. A speckle pattern can be obtained from a single pulse of intense coherent X-rays before causing irreversible damage in the sample.

## 1.2 Coherent Hard X-ray Beamline Team

In this section, an overview of the CHX team (as of Summer 2009) is given, as well as a brief description of the scientific and instrumentation interests of the NSLS-II Beamline Scientists, the management and engineering support and members of the Beamline Advisory Team (BAT).

### Beamline Scientists

**Andrei Fluerașu**, Associate Physicist, NSLS-II, CHX Group Leader

Dynamics in non-equilibrium and driven systems – e.g., gels and glasses under flow/shear; Applications of XPCS,  $\mu$ -beam SAXS in biophysics; Speckle Visibility Spectroscopy; Beamline optics and coherence preservation; Pushing the signal-to-noise ratio in XPCS, CDI by optimizing the beamline layout; X-ray detectors; Controls and data acquisition; Statistical analysis of speckle-based methods

**Lutz Wiegart**, Assistant Physicist, NSLS-II

Structure and dynamics at liquid surfaces and interfaces; CDI in biological systems; Bulk dynamics associated with self-assembly of organic nanotubes; Solution scattering; Sample environments; Experimental setups adapted to coherent x-ray scattering

**Lonny Berman**, Physicist, NSLS (MOU)

Macromolecular and protein crystallography; Applications of coherence for imaging and studies of dynamics; Beamline optics and beamline design; Coherence preservation by beamline optics; Restoring the coherent wavefront with adaptive optics.

### **NSLS-II Management and Engineering Support**

**Qun Shen**, Director, Experimental Facilities Division, NSLS-II, BNL

**Andy Broadbent**, Beamline Manager, Experimental Facilities Division, NSLS-II, BNL

**Oleg Chubar**, Beamline Scientific Support, XFD, NSLS-II, BNL

**Konstantine Kaznatcheev**, Beamline Scientific Support, XFD, NSLS-II, BNL

**Mary Carlucci-Dayton**, Mechanical Engineer, XFD, NSLS-II, BNL

**Viswanath Ravindranath**, Mechanical Engineer, XFD, NSLS-II, BNL

Much of the required design and engineering work is performed in a “centralized” fashion, with the whole suite of six project beamlines and the following 50+ beamlines in sight. This routinely involves tight collaborations between the scientific and engineering staff across the whole Experimental Facilities Division and even the whole NSLS-II project. The whole design of the baseline Front Ends was performed, for instance, by the Mechanical Engineering Group in the Accelerator Division. The beamline also uses resources from the same group for tasks such as FEA simulations, synchrotron and bremsstrahlung ray tracing, etc.

The Beamline Advisory Team is not only formed by world experts in XPCS but also by scientists who invented and pioneered this technique. The scientific and technical interest of all the BAT members cover a wide range of topics in condensed matter physics, biophysics, instrumental design, and the development at world-class facilities.

### **Beamline Advisory Team (BAT)**

**Robert Leheny**, Associate Prof., John Hopkins Univ. (spokesperson)

**Karl Ludwig**, Professor, Boston University

**Laurence Lurio**, Associate Professor, Northern Illinois University

**Simon Mochrie**, Professor, Yale University

**Lois Pollack**, Associate Professor, Cornell University

**Aymeric Robert**, Instrument Scientist, LUSI/LCLS, SLAC

**Alec Sandy**, Physicist, 8-ID, APS, ANL

**Oleg Shpyrko**, Assistant Professor, University of California San Diego

**Mark Sutton**, Professor, McGill University

## 2 BEAMLINE LAYOUT

### 2.1 Overview

Key to performing XPCS measurements is a (partially) coherent x-ray beam. The coherence of a photon beam has two components: transverse or lateral coherence and longitudinal or temporal coherence. For a synchrotron source of x-rays, with an approximately Gaussian intensity distribution, far from the source, the transverse “one-sigma” coherence lengths in the horizontal (x) and vertical (z) direction are  $\xi_x, \xi_z = \lambda L / 2\pi\sigma_{x,z}$ . Here  $\lambda$  is the x-ray wavelength, and  $\sigma_{x,z}$  are the “one-sigma” source sizes in the horizontal and vertical directions, respectively  $\sim 35 \mu\text{m}$  and  $\sim 4 \mu\text{m}$  at NSLS-II (assuming a fully damped source), and  $L$  is the source-to-sample distance.

It follows that, for a photon energy of  $E=8\text{keV}$ , for instance, and at a distance  $L=45\text{ m}$  from the source, near the current sample location in the CHX layout, this leads to one-sigma transverse coherence lengths in the horizontal and vertical directions of  $\xi_x=31.7 \mu\text{m}$  and respectively  $\xi_z=277.5 \mu\text{m}$ . These are both too large as the spot size has to be small enough to enable speckle detection. As a consequence, the beam has to be focused to smaller sizes in both directions. The maximum spot size that allows resolving individual speckles is determined by the detector resolution and/or working distance. Assuming a detector pixel size of  $80 \mu\text{m}$  and a maximum detector distance of  $R=15\text{ m}$  (both limited by practical and/or technological limits), the spot size on the sample ( $D$ ) corresponding to a speckle size  $S \sim 100 \mu\text{m}$  is given by  $D = \lambda R/S = 23.25 \mu\text{m}$ . Maximizing the XPCS signal-to-noise ratio (SNR) requires a spot size of “a few” one-sigma coherence lengths. It turns out that a good estimate for an “optimal” spot size is the full-width at half maximum ( $\text{FWHM} = \sqrt{2\ln 2} \sigma \approx 2.35\sigma$ ) hence the one-sigma spot size corresponding to the speckle size mentioned above is  $\sim 10 \mu\text{m}$ . In order to perform XPCS in a SAXS geometry, the beamline optics should thus create a one-sigma spot size of  $10 \mu\text{m}$  at the sample location. This can be achieved via focusing in numerous ways. In our current design, a focusing instrument consisting in a combination of Beryllium Compound Refractive Lenses (CRL) is placed in the pink beam around  $\sim 29\text{--}30\text{ m}$  from the source in order to provide the required “gentle” focusing. One possible layout that will provide the required beam size is shown in Figure 2. If a 2:1 demagnification geometry is used in the vertical direction with a lens placed around  $y=29.4\text{ m}$ , this will create a secondary source of  $2 \mu\text{m}$  at  $44.2\text{ m}$  which, in turn will give a one-sigma coherence length at the sample location ( $45\text{ m}$ ) of  $\xi_z \sim 10.36 \mu\text{m}$  (Figure 2a). Two possible layouts are presented (Figure 2b and 2c) to achieve a similar horizontal beam size. In the first one, a 1:1 lens around  $y=30\text{ m}$  is used to create a virtual source of  $35 \mu\text{m}$  near the detector location at  $y=60\text{ m}$ . The horizontal coherence length determined by this source at the sample location is  $\xi_x \sim 10.57 \mu\text{m}$  and, since the virtual source is behind the sample, this can be obtained by closing the horizontal gap of the secondary slits SS2. Alternatively, if a 3:1 focusing is used in the horizontal direction, a secondary source of  $\sim 11.7 \mu\text{m}$  is created at  $40\text{ m}$  from the source which will result in the same transverse horizontal coherence length of  $\xi_x \sim 10.57 \mu\text{m}$   $5\text{ m}$  downstream, near the sample location (Figure 2c).

By keeping the sample location close to the source, the detector distance can be sufficiently large to allow resolving relatively small speckles in XPCS-SAXS experiments. The speckle size  $S$  for a sample-detector distance  $R$  is given by  $S = \lambda R/D$ . In the current design,  $R$  can be as large as  $15\text{ m}$ , but can also be easily changed to any other shorter distances. With a one-sigma transverse coherence length of  $\sim 10 \times 10 \mu\text{m}^2$ , as in the example above, the FWHM optimal beam size for XPCS experiments is about  $23.5 \times 23.5 \mu\text{m}^2$  and, at  $R=15\text{ m}$ , this leads to a speckle size of  $\sim 92.4 \mu\text{m}$ . The SNR in the correlation functions increases when the speckles underfill the detector pixels (even though the optical contrast decreases), hence a detector with pixels of  $\sim 100 \mu\text{m}$  or smaller would be optimal. Our current expectation is that it will be possible to develop a fast (e.g.,  $1\text{--}10\text{ MHz}$ ) detector with individual counters and possibly correlators for each pixel while keeping the pixel size around  $\sim 80 \mu\text{m}$  (D. P. Siddons et al., *unpublished*), and this will be suitable for XPCS experiments with the current beamline layout, provided their size will allow to cover a large-enough  $q$ -range.

For CDI experiments, the optical contrast will have to be maximized by adjusting the incident beam to a one-sigma size or smaller. In this case the speckles (at the same maximum available distance of  $R=15\text{ m}$ ) will exceed  $\sim 220 \mu\text{m}$ ,

which matches the assumed pixel size of  $80\text{ }\mu\text{m}$  and required oversampling conditions. Often the “effective” beam size will be even smaller, as for isolated samples (e.g. a frozen cell) this is determined by the size of the object rather than the beam size. The optimal detector for CDI will be an integrating or photon counting detector with a high dynamic range and small-enough pixel size. Such detectors may become commercially available during the construction of the CHX beamline (e.g. Pilatus II).

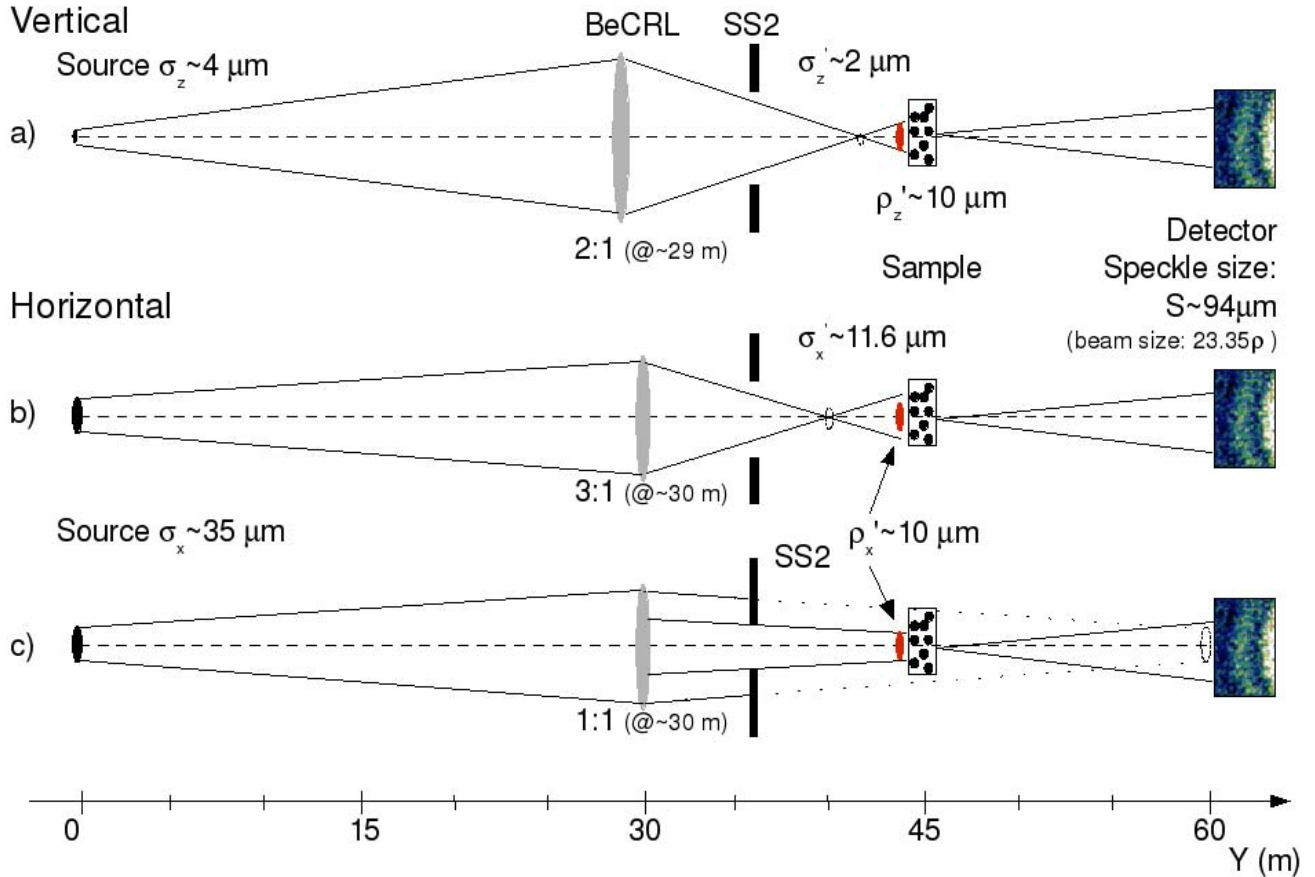


**Figure 2** Possible optical layout for XPCS in a SAXS geometry. a) Vertical: A 2:1 focusing optics (represented here as a lens) placed around  $y=29.4\text{ m}$  is used to create a  $\sim 2\text{ }\mu\text{m}$  secondary source at  $\sim 44.2\text{ m}$ . This new source will yield a coherence length of  $\xi_x \sim 10.4\text{ }\mu\text{m}$  at the sample location, ( $y=45\text{ m}$ ). b) Horizontal: A similar scheme, with a 3:1 lens placed at  $y=30\text{ m}$  is used to achieve a horizontal coherence length at the sample location of  $\xi_z \sim 10.6\text{ }\mu\text{m}$ . c) Horizontal: Alternatively, a 1:1 lens can be used to create a virtual source downstream of the sample around  $y=60\text{ m}$ . The corresponding coherence length at the sample location is still  $10.6\text{ }\mu\text{m}$ , and the horizontal beam size can be limited by one of the available sets of secondary slits.

Wide-angle XPCS experiments will require much smaller beam sizes due to the more important effect that the finite longitudinal coherence length has on the speckle contrast in this geometry (see below) and to a much smaller detector distance limited by obvious practical reasons. A beam size of a few micrometers will be obtained in this case using horizontal and vertical focusing of the monochromatic beam with elements such as silicon kinoforms placed closer to the sample.

In addition to the transverse coherence, XPCS requires also partial longitudinal coherence (S. Mochrie, *unpublished*) The longitudinal coherence length of the beam is given by its monochromaticity  $\Lambda = \lambda(E/\Delta E)$ , where  $E$  is the photon energy, and  $\Delta E$  is the full-width-at-half-maximum (FWHM) of the energy spectrum. Partial longitudinal coherence requires that the optical path length difference ( $\delta$ ) between x-rays scattered from different parts of the sample should

not be more than a few times  $\Lambda$ . For a transmission geometry, there are two contributions to  $\delta$ . The first one, which arises because of a non-zero width ( $D$ ) of the illuminated portion of the sample within the scattering plane, is

$$\delta_D = 2D \frac{Q}{k} \sqrt{1 - \frac{Q^2}{k^2}}.$$

The second comes from the non-zero sample thickness ( $W$ ) and is

$$\delta_W = 2W \frac{Q^2}{k^2}.$$

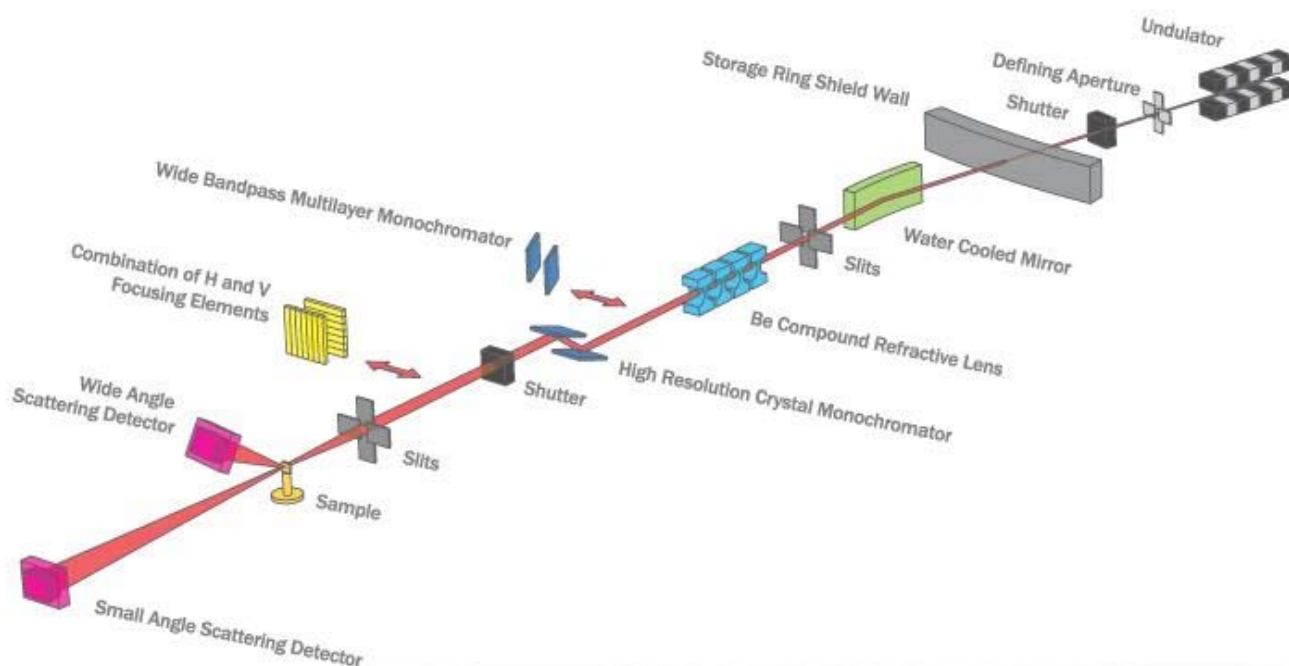
Usually,  $\delta_W$  is small for typical values of  $W$  and may be neglected. By contrast,  $\delta_L$  becomes comparable to  $\Lambda$  as  $Q$  reaches a maximum acceptable value. For a Si(111) monochromatic beam with  $E/\Delta E \approx 10^4$ , and a “typical” XPCS-SAXS transverse beam size  $D \approx 20 \mu\text{m}$  the maximum value of  $Q$  is about  $1.5 \text{ nm}^{-1}$ . As this is higher than needed in most SAXS experiments, many of them can be performed using a “pink” beam with  $E/\Delta E \approx 10^2$ , which limits the  $Q$  range to below  $Q_{\text{max}} \approx 1.5 \times 10^{-2} \text{ nm}^{-1}$ . From this analysis it is clear that longitudinal coherence requirements are more stringent in XPCS-WAXS. With the same Si(111) crystal and a beam size  $D \approx 1 \mu\text{m}$ , the maximum value of  $Q$  becomes  $Q_{\text{max}} \approx 3.2 \text{ \AA}^{-1}$ . This also shows that a higher crystal cut with a smaller bandwidth will be beneficial for many WAXS experiments. The design of the CHX double crystal monochromator will allow the choice of several Si crystals.

The working energy range at the CHX beamline should be as large as possible, in order to offer a good flexibility in designing different experiments. A lower working energy will maximize the coherent flux which is given by  $\lambda^2 B/4$  (note:  $B$  itself depends on energy and is larger at smaller energies). However, higher energies will help to reduce beam damage, allow experiments with thicker samples, allow working near or above several potentially useful edges (Mn, Fe, Co, Ni, Cu ...) etc. The proposed energy range for the CHX beamline is 6-16 keV.

The beamline layout and 3D model of the proposed CHX beamline can be seen in Figure 3. A long, pink beam compatible experimental hutch (EH) will allow a max sample-detector distance of  $\sim 15 \text{ m}$  for SAXS experiments. The sample will be held on a versatile diffractometer which will allow also WAXS. Even though it is expected that in general an experiment will be performed either in SAXS or WAXS geometry, this arrangement opens the possibility to perform simultaneous WAXS and SAXS in certain situations (e.g., simultaneous measurement of capillary wave dynamics and structure formation on liquid surfaces).

The white-beam compatible optics hutch (OH) should be short in order to minimize the source-sample distance, but long enough to provide enough clearance to stop the bremsstrahlung while letting the pink beam deflected by a horizontal white-beam mirror go through to the EH. A choice of either a vertically deflecting “channel-cut type” monochromator offering a choice of Si crystals - e.g. Si(111), Si(311) - or a double multilayer monochromator will provide the choice of working with a high resolution monochromatic beam or a lower resolution pink beam.

a)



b)

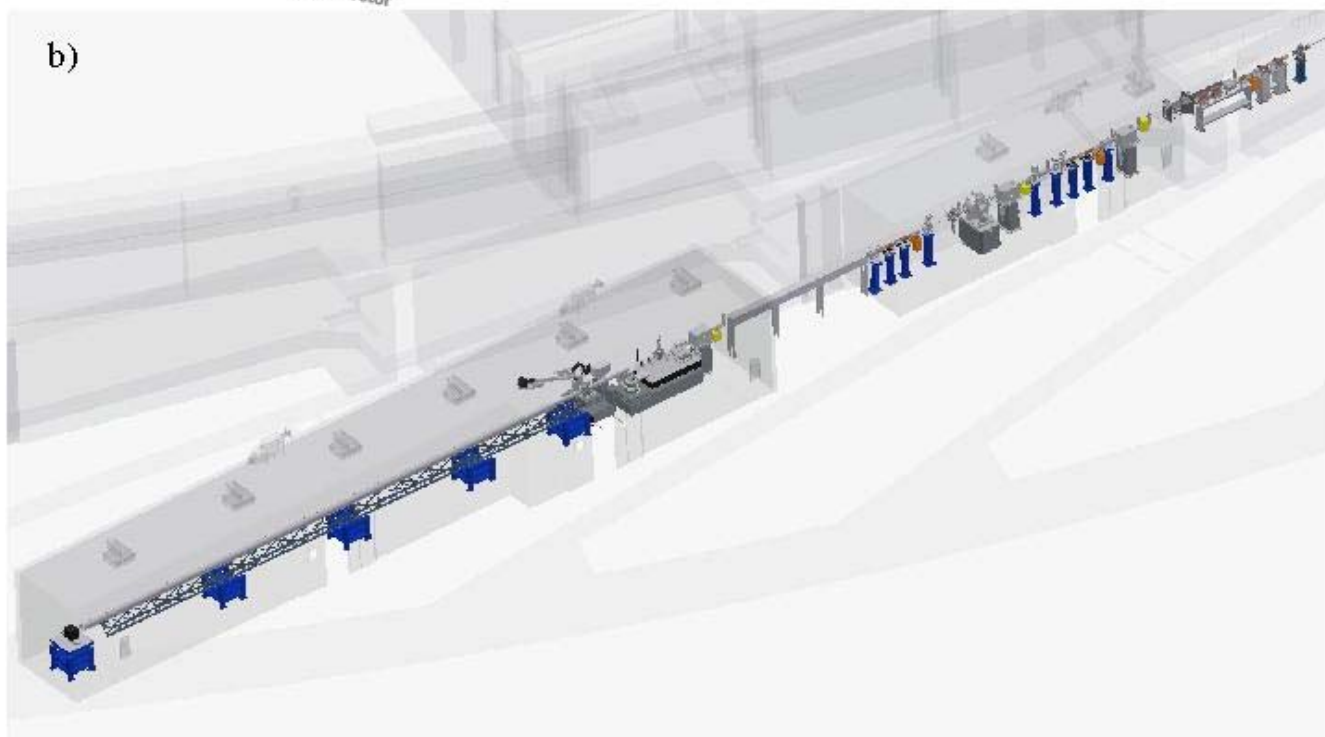


**Figure 3** a) Schematic representation (not to scale) showing the optic layout of the CHX beamline; b) 3D perspective of the beamline including the Front End (FE), optics hutch (OH) and the experimental hutch (EH), which exceeds 20 m in length.



## 2.2 Insertion Device

Since the XPCS SNR is proportional to the source brilliance, the CHX beamline will be built on a low-beta straight section which yields the highest brilliance possible at NSLS-II. The insertion device, a 3m long U20 in-vacuum undulator (IVU) is the brightest of any devices in the NSLS-II baseline configuration. Its specifications can be seen in Table 1. The beamline will cover an energy range from 6keV to 15keV and will work most typically on the 5<sup>th</sup> harmonic of the U20 IVU but also on the 3<sup>rd</sup>, for lower energies, or the 7<sup>th</sup> harmonic for the higher energy end of the covered spectrum. For most working energies, the brilliance of the CHX source will exceed the 10<sup>21</sup> ph/s/0.1%BW/mm<sup>2</sup>/mrad<sup>2</sup> level, at least one order of magnitude higher than APS or ESRF. This unprecedented increase in source brightness is due to the very small emittance of the storage ring achieved with several damping wigglers (DW).

**Table 1.** Basic Parameters of NSLS-II U20 IVU on a Low-Beta Straight Section (Storage Ring Operating at 3 GeV and 500 mA).

U20	
Type	IVU
Photon energy range [keV]	Hard x-ray (1.9–20)
Type of straight section	Low- $\beta$
Period length, $\lambda_U$ [mm]	20
Total device length [m]	3.0
Number of periods	148
Minimum magnetic gap [mm]	5
Peak magnetic field strength in linear mode, B [T]	1.03
Max $K_y^*$ , linear mode	1.81
Peak magnetic field strength in circular mode, B [T]	
Max $K_h = K_y^*$ , circular mode	
Minimum $h\nu$ fundamental [keV]	1.62
$h\nu$ critical [keV]	
Maximum total power [kW]	9.1
Horizontal angular power density [kW/mrad]	
On-axis power density [kW/mrad <sup>2</sup> ]	65.4

\* $K = 0.934 B[T] \lambda_U[cm]$ ; effective K values listed

The fully-damped horizontal emittance value of 0.5 nm rad is assumed in all the parameters calculated by the NSLS-II Accelerator Systems Division (ASD) and reported here. This is the performance value for the NSLS-II storage ring when operating with a full complement of eight 7m damping wigglers. The initial emittance value will be greater than this value, owing to operation with fewer damping wigglers. The one-sigma electron beam size –  $\sigma_{electron}$  – of the NSLS-II undulator is shown in Table 2 (source size and divergence in horizontal and vertical direction).

The diffraction-limited, “natural” photon beam size  $\sigma_{photon}$  is given by

$$\sigma_{photon} = \frac{1}{4\pi} \sqrt{2L\lambda}.$$

This is the size of a diffraction-limited photon beam for a zero emittance (and therefore zero size) electron beam. One measure of the effective photon beam size,  $\sigma_{eff}$ , is given by the quadrature sum of the electron ( $\sigma_{electron}$ ) and photon ( $\sigma_{photon}$ ) contributions:

$$\sigma_{eff} = \sqrt{\sigma_{electron}^2 + \sigma_{photon}^2}.$$

**Table 2.** Electron Beam Size and Divergence at the Center of a Low-Beta Straight Section of the NSLS-II Storage Ring.

Type of source	Low- $\beta$ straight section (6.6m)
$\sigma_h$ [ $\mu\text{m}$ ]	31.8
$\sigma_h'$ [ $\mu\text{rad}$ ]	15.7
$\sigma_v$ [ $\mu\text{m}$ ]	2.9
$\sigma_v'$ [ $\mu\text{rad}$ ]	2.8

Similarly, the diffraction-limited, “natural” photon beam angular divergence  $\sigma'_{\text{photon}}$  is given by

$$\sigma'_{\text{photon}} = \sqrt{\frac{\lambda}{2L}},$$

and the effective photon beam angular divergence  $\sigma'_{\text{eff}}$  is again given by the quadrature sum of the electron ( $\sigma'_{\text{electron}}$ ) and photon ( $\sigma'_{\text{photon}}$ ) contributions:

$$\sigma'_{\text{eff}} = \sqrt{\sigma_{\text{electron}}^2 + \sigma_{\text{photon}}^2}.$$

The effective photon beam size and angular divergence are shown in Figure 4 for two of the NSLS-II baseline insertion devices—EPU45 (red) and the CHX insertion device, U20 IVU (blue). The gray lines (straight, on a log-log graph) show the “natural” diffraction-limited photon beam size and angular divergence. The resulting brightness of all the NSLS-II baseline radiation sources is shown in Figure 5.

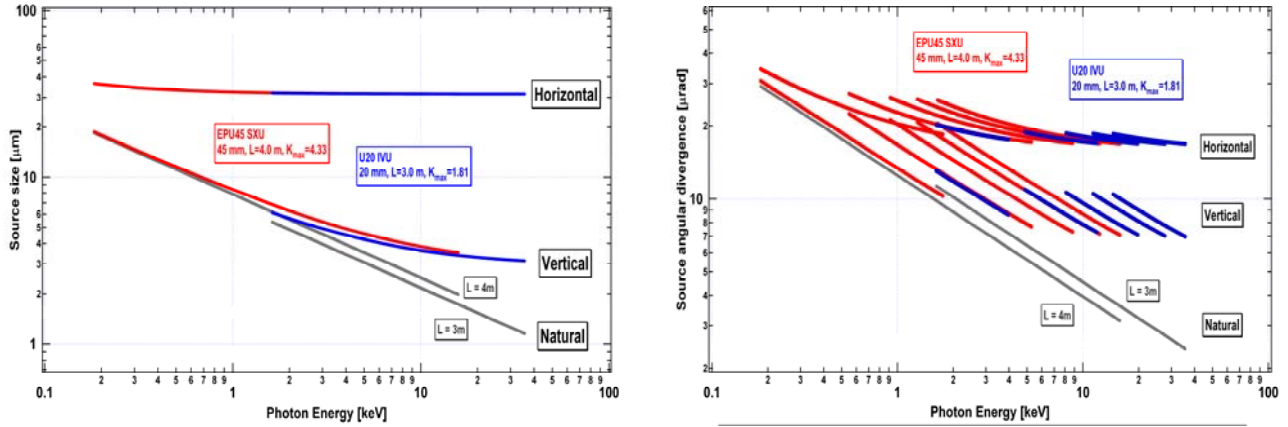


**Figure 4.** Vertical and horizontal photon source size and angular divergence for EPU45 soft x-ray undulator (red) and U20 IVU (blue). The gray lines show the calculated diffraction-limited size and angular divergence (see text).

To avoid unnecessarily increasing the heat load on the beamline optics, the CHX instrument will use only a small part of the beam, corresponding to one or “a few” transverse coherence lengths. This will be defined with the high heat load primary slits located at about 20m from the source, in the front end (FE). An estimate of the FWHM coherent beam size at this distance from the source is given in Table 3. The one-sigma coherence length has been estimated using  $\xi_x, \xi_z = \lambda L / 2\pi / \sigma_{x,y}$  and the aperture size was considered to be FWHM  $\sim 2.35\sigma$  in order to compromise between an increased SNR and a lower contrast with a larger beam.



**Table 3.** Coherent beam size – FWHM =  $2.35\sigma$  – at the primary slits. Selecting a small beam size, corresponding to only “a few” coherence lengths, has clear advantages in terms of heat load on all the downstream elements.

E (keV)	6	8	10	12	16
$\lambda$ (Å)	2.06	1.55	1.24	1.03	0.77
$\zeta_z$ (μm)	447.3	335.5	268.4	223.6	154.2
$\zeta_x$ (μm)	44.7	33.55	26.8	22.4	17.6

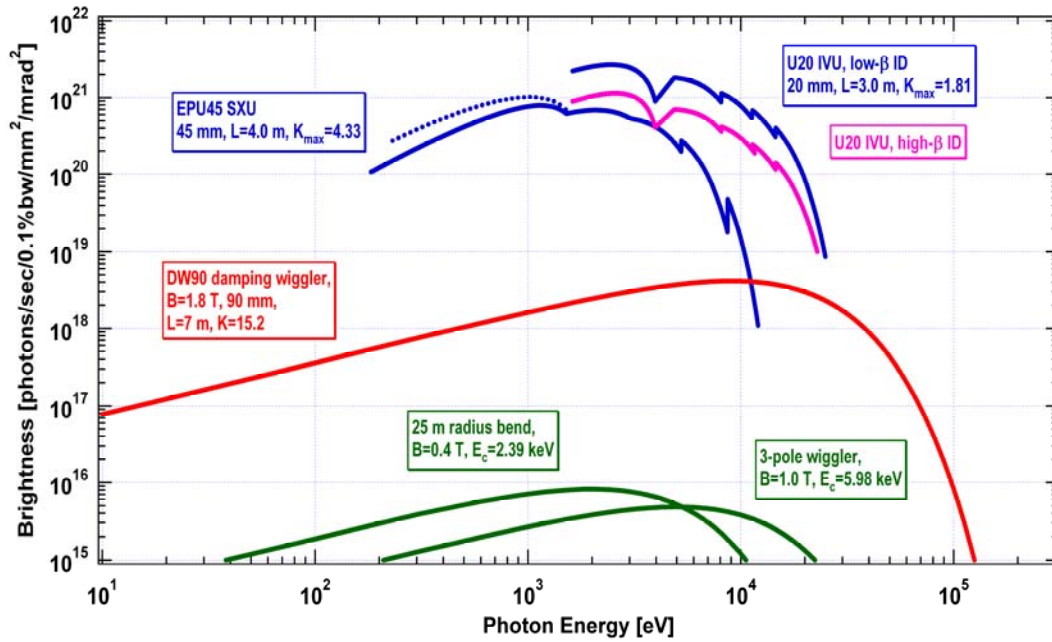


**Figure 5.** Brightness vs. photon energy for the baseline radiation sources at NSLS-II. Ring parameters: 3.0 GeV,  $I=0.5$  A,  $\varepsilon_h=0.5$  nm,  $\varepsilon_v=0.008$  nm, energy spread=0.001; Straight section, low- $\beta$ :  $\beta_h=2.02$  m,  $\beta_v=1.06$  m.

The filling modes and bunch uniformity will be of a particular importance for the CHX beamline. It is estimated that, in order to have clean baseline for the correlation functions that will enable measurements of sub-microsecond dynamics, the NSLS-II storage ring should provide a high current (500 mA) quasi-DC source with at least 4/5 of the buckets filled and the remaining, ion clearing buckets uniformly distributed across the ring. We estimate that a bunch-to-bunch uniformity better of 1% will lead to a structure in the correlation function safely below the noise level, while a 10% variation would be detectable in data with good statistics (hence, will require correction). More details about various synchrotron filling modes are given in section 4, Special Beamline Requirements.

## 2.3 Front End

The CHX beamline will use a standard NSLS-II front end configuration (see Figure 6). The key element in addition to the beam position monitors that will provide information about the transverse and angular position of the photon beam, a fixed aperture and a number of collimators, will be a set of X-Z high heat load slits with 1 μm precision/accuracy. These slits, also shown in Figure 6, are based on the design provided by the Mechanical

Engineering Group in the Accelerator System Division (ASD) and are described in more details, in the general front end section of this conceptual design report.

The slits are made out of a water cooled GlidCop body with stainless steel adapters and flanges. A set of tungsten corners will allow defining the beam (e.g., top, right with the first unit and bottom, left with the second unit). Each unit will be mounted on a motorized X-Z stage. The slit design (e.g. angle of the tapered profile in the GlidCop bodies and shape/geometry of the beam-defining Tungsten corners) has been optimized to cope with the high power load associated with white beam operation. They are a critical element in the beamline layout since by absorbing several kW of incident power, the flux transmitted to the downstream optics will be greatly reduced. For instance, with the slits set to a “default” 500  $\mu\text{m}$  (vertical) and 100  $\mu\text{m}$  (horizontal) which is still larger than the coherence length at any wavelength (see Table 3), and an estimated peak power of  $\sim 90 \text{ W/mm}^2$  in the central cone of the U20 undulator (which is quite uniform over this reduced spatial range), the total power incident on the next optic element, in this case a horizontally deflecting flat mirror is only on the order of 4.5 W.

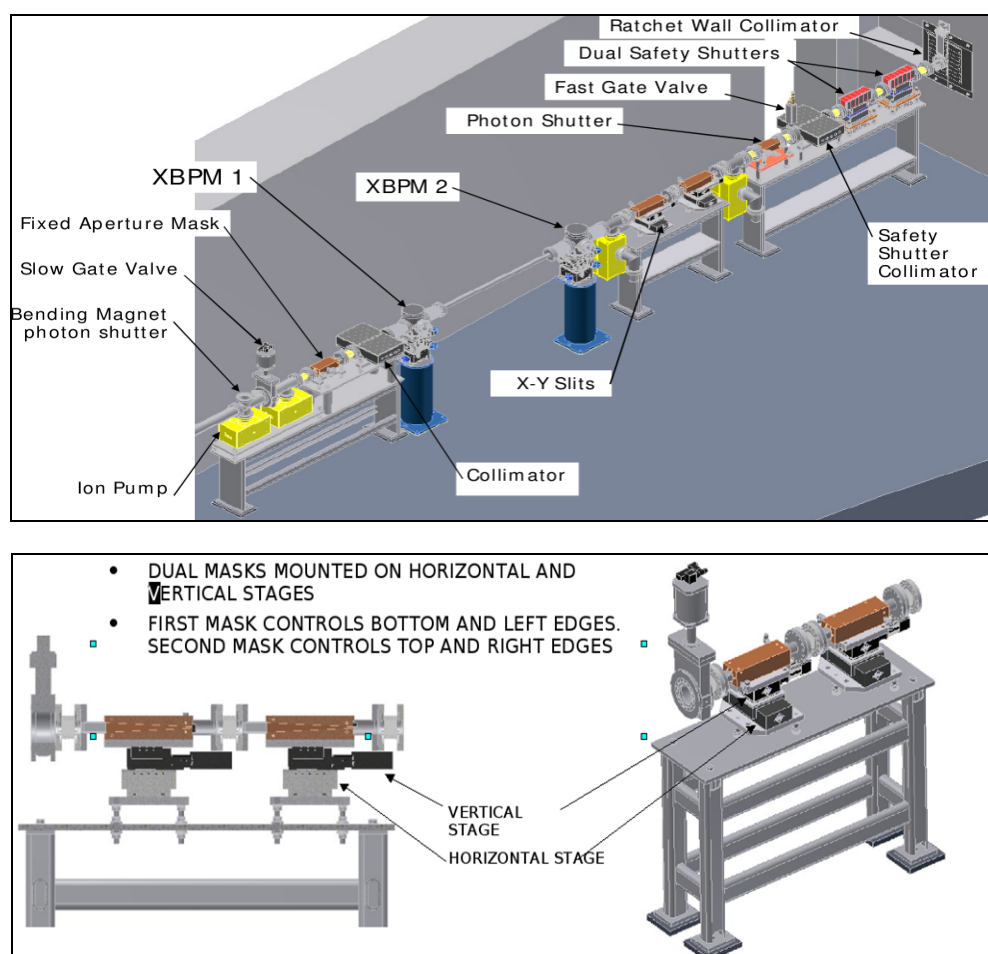


**Figure 6.** Front-End configuration and the high heat load X-Z precision slits, which will be used to limit the amount of power incident on the beamline optics by retaining only a few coherent modes of the photon beam.

The scannable primary slits will determine the size of the beam incident on the next optical element, which is the fixed-angle horizontally deflecting mirror (a complete description can be found below in the Optical layout section). The power density on the mirror is low due to the relatively small incidence angle leading to a large footprint, hence water-cooling will be sufficient. However, since even small slope errors of a few  $\mu\text{rad}$  are considered to be too large, it is anticipated that the footprint of the beam on the mirror will have to be (significantly) larger than the final size of the coherent beam. It is even likely that the best performance will be obtained with a fully illuminated mirror and the coherent beam defined only further downstream by the secondary slits. For this reasons, the optical layout described below features two sets of high heat load slits placed before and after the mirror. This configuration offers

all the required heat-load management features and maximizes the flexibility for an optimal tuning of the beamline performance.

## 2.4 Optical Layout

The main consideration taken into account in the optical design of the CHX beamline is coherence preservation. The number of windows is reduced to a minimum and the optic elements will be polished to the best available figures. An R&D program devoted to coherence preservation by mirrors and multilayers is on-going at NSLS-II. The main goal is to identify the vendors and polishing methods that will allow optics with slope errors of 100 nrad or better.

The mechanical design of all critical elements will pay a particular attention to the overall stability. All the major elements in the proposed beamline layout are described below starting from the Front End ratchet wall and proceeding downstream.

### White Beam Mirror

The first optic element in the beamline layout (apart the beam-defining X-Z slits placed in the Front End) is a horizontally-deflecting, nominally flat, white beam mirror. For simplicity and stability reasons, the incidence angle on the mirror will be fixed. A vertical translation will allow the choice between several stripes on the mirror surface. The presence of the deflecting mirror allows the possibility to stop the direct bremsstrahlung radiation in the optics hutch hence eliminates the need to build a (cost prohibitive!) white-beam compatible experimental hutch. In addition, it will also help by reducing the thermal load on the downstream optical elements and by lowering the radiation background in the Experimental Hutch. Finally, the total-reflection mirror provides a simple way to achieve high harmonic rejection in certain cases.

Increasing the angle of incidence is favorable for providing a larger deflection angle hence more room for collimators, beam stops, etc. However, decreasing the incidence angle will increase the mirror reflectivity. In the current layout, an incidence angle of 0.18 deg (3.14 mrad) will allow work with a bare Si (cutoff energy 10.4 keV) stripe for energies below ~9–10 keV or with a Rh-coated stripe (cutoff energy ~20.8 keV) for higher energies.

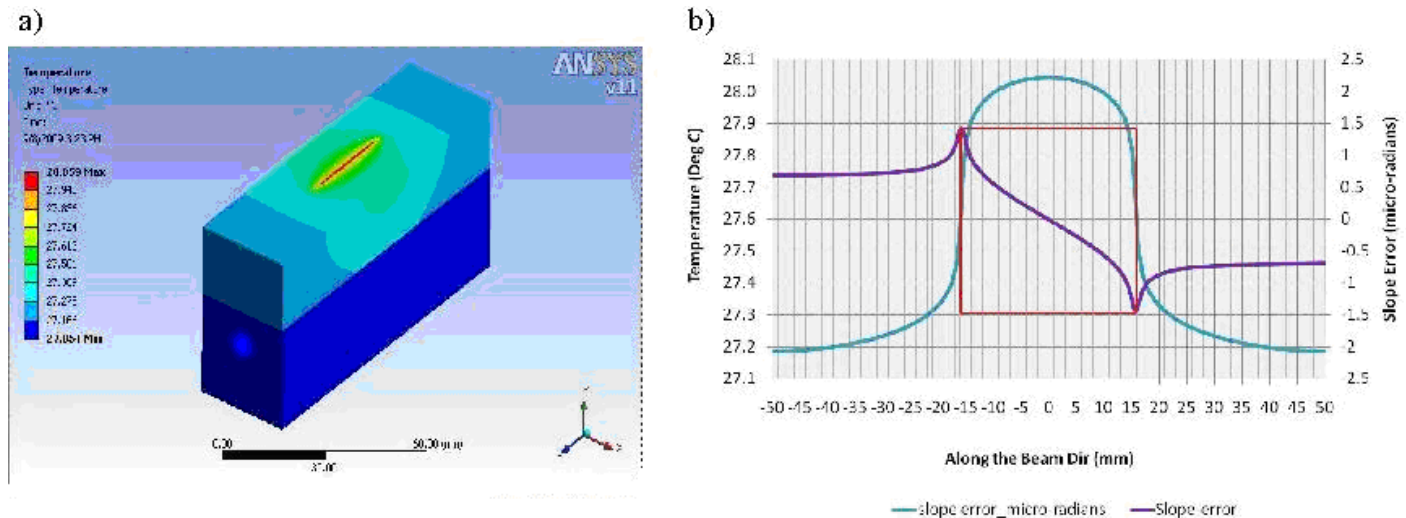


**Figure 7.** Finite Element Analysis for the white beam mirror assuming an indirect “back cooling” geometry. The temperature raises by less than 1°C and the maximum slope error within a “region of interest” corresponding to the coherence lengths will not exceed ~0.2  $\mu\text{rad}$ .

With the small beam size at the CHX beamline and the horizontal reflection geometry, the footprint of the beam on the mirror will be quite small, e.g., the same “default” 500  $\mu\text{m}$  (V) x 100  $\mu\text{m}$  (H) incident beam will give a footprint of ~500  $\mu\text{m}$  (V) x 3 cm (H) on the mirror. The power density will also be low, less than 0.3 W/mm<sup>2</sup> in this case, and can be handled by indirect water cooling of the mirror (Figure 7).

The polishing of the mirror surface and overall flatness will be of utmost importance for the coherence preservation properties of this element. In order to avoid affecting the speckle structure coming from the sample and given the fact that angular speckle sizes can be as small as  $\sim 3 \mu\text{rad}$ , it is estimated that slope errors well below  $1 \mu\text{rad}$  (ideally  $100\text{--}200 \text{ nrad}$ ) will be required at the CHX beamline. Obviously, the heat-induced deformations should also be kept within the same range.

### **Secondary Slits**

A second set of water-cooled adjustable slits will follow in order to allow for collimation and further reduction of the power load on downstream components. Since the power densities can be locally high, this will also be a high heat load set of slits, based on the same design as the primary slits placed in the Front End.

### **Be CRLs for Vertical Focusing**

All the XPCS experiments performed at the CHX beamline will require focusing in order to take advantage of the full transverse coherence lengths. This will be done using a selection of parabolic Be Compound Refractive Lenses (CRL) for vertical and horizontal focusing.

The Be CRLs are preferred over other possible focusing elements (mirrors, kinoforms, etc) because of their high reliability, tolerance to surface imperfections, and simplicity of use. Similar parabolic Be CRLs have been in regular user operation for several years at beamline ID10, ESRF. The vast majority of experiments performed there are using vertical focusing and the overall performance of the beamline improved by at least one order of magnitude with their installation.

The lenses that we plan to use – 1D focusing with cylindrical symmetry and parabolic profiles – are not available at this time, but we believe collaborations with groups that are world leaders in the fabrication of Be CRLs should enable us to obtain first prototypes for testing on a reasonably short time scale.

Preliminary heat load analysis performed using various FEA models have shown encouraging evidence that it will be possible to use them in white (or pink) beam if the (water) cooling is applied close-enough to the lenses. It is believed that it will be possible to keep the maximum operating temperature around  $100\text{--}150 \text{ deg}$  and the mechanical stresses around or below the yield stress to plastic deformation.

### **Monochromator(s)**

Most of the experiments at the CHX beamline will be performed using a vertically deflecting double crystal monochromator (DCM). The monochromator will be designed to achieve angular stability better than  $100 \text{ nrad}$  and for this reason the vertical offset between the two crystals will be kept low – i.e. about  $5\text{--}6 \text{ mm}$ . The design will be simple and robust with a “channel-cut type” crystal cage made from two crystals cut from the same Si ingot and a piezo actuator adjusting the angular position of the second crystal to compensate for thermal offsets. In order to maximize stability the mechanical design will minimize the use of ball bearings and will mainly be based on flexure couplings.

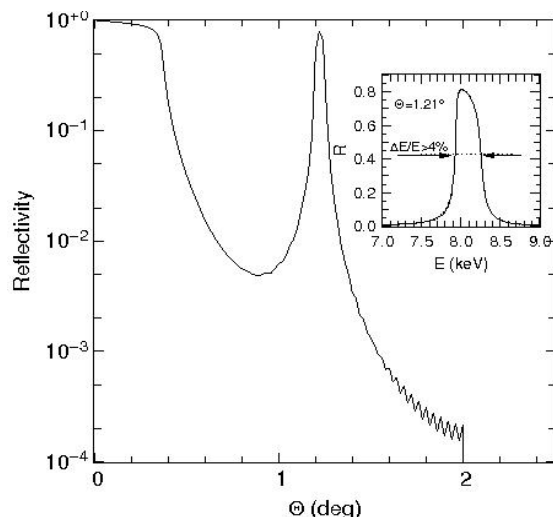
The slope errors associated with thermal deformations of the first crystal should also be kept as low as the other “figures of merit” e.g., slope errors of the mirror or vertical stability and for this reason the DCM will use liquid nitrogen cryogenic cooling. The details of the FEA thermal analysis that proved that water cooling would not be sufficient are presented in the next section.

The fine monochromatic resolution obtained with a crystal monochromator is sometimes unnecessary in XPCS experiments working in a small-angle (SAXS) scattering geometry. In such cases, the use of broader bandwidth diffractive optics such as multilayers (ML) provide a good practical means to obtain more intense coherent beams - essentially “pink beams” - with excellent harmonic rejection efficiencies.

Here is an example of an experimental strategy that could provide a pink beam operation mode at a typical energy for XPCS experiments -  $E=8\text{keV}$ . The ML structure chosen in this simulations is a series of  $N=200$   $\text{WSi}_2/\text{Si}$  bilayers. Such structures are grown in the optics group at NSLS-II and have already been tested in coherent X-ray beams (see below). They are also commercially available from a number of vendors.

The simulated reflectivity curve of this structure for a photon energy of 8 keV can be seen in Figure 8. The peak value for the reflectivity is obtained for an incidence angle of 1.208 deg,  $R=0.81$ . This matches very well the measured reflectivity from a very similar ML structure (Figure 9). A sputtering deposition chamber that will allow growing such structures in-house will be installed and commissioned in the NSLS-II R&D laboratories in the very near future and it is in our plans to grow similar structures in-house.

**Figure 8**  
Simulated reflectivity from a  $\text{WSi}_2/\text{Si}$  multilayer structure for a photon energy of 8 keV. The parameters considered in this simulations are: multilayer period  $d=3.8$  nm  $r=0.7$  (Si layer thickness / period), thickness of inter diffusion layer  $s=4$  Å, number of periods  $N=200$ . The inset shows the bandwidth of the 1<sup>st</sup> order  $E=8$  keV reflection peak at an incidence angle of 1.208 deg.



The maximum intensity at 8 keV, will be obtained from the 5<sup>th</sup> harmonic of the U20 undulator. The approximate bandwidth of the undulator radiation is than  $\Delta E/E=1/nN=1/750$ , with  $n=5$  for the 5<sup>th</sup> harmonic and  $N=150$ , the number of the U20 undulator periods. This approximation only takes into account the pulse length of light from a single electron resulting from the difference in travel time through the undulator between electron and photon. The results of a full calculation, taking into account diffraction effects resulting from the finite source size and angular spread is shown in Figure 10.

**Figure 9**  
Measured reflectivity ( $E=8.04$  keV, Cu-K $\alpha$  rotating anode) from a  $\text{WSi}_2/\text{Si}$  multilayer structure (parameters shown on the graph).

*Courtesy of Ray Conley*

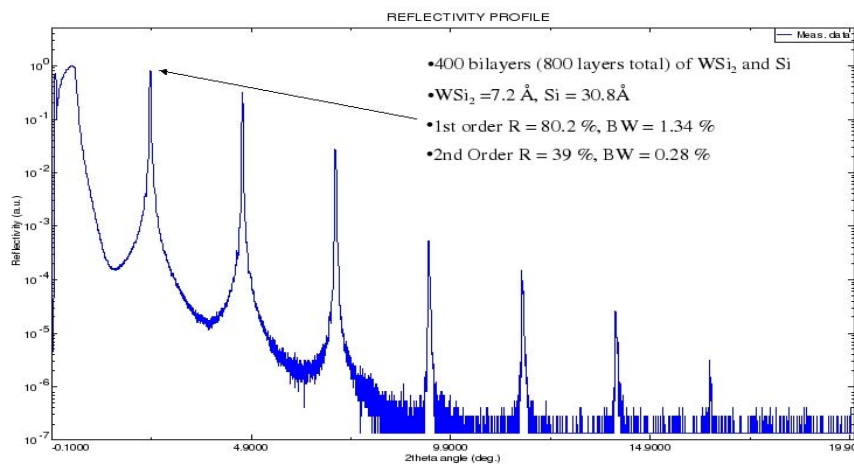
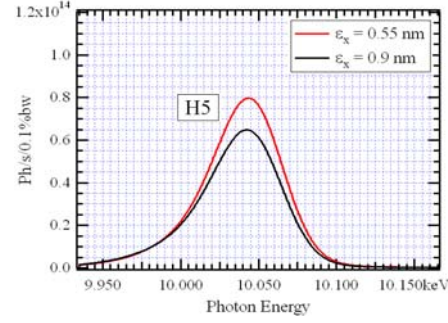




**Figure 10.** Line shape of U20 5<sup>th</sup> harmonic calculated for  $K=1.5$  and a low- $\beta$  straight section. The red curve was calculated assuming a fully damped (8 DWs) source while the black one shows the “day one” line width with only 3 DWs in the SR lattice.

*Courtesy of Oleg Chubar*



It is thus quite clear from this analysis that with the long U20 and high harmonics that will typically be used at the CHX beamline, the undulator line width will always be smaller than the bandwidth of the multilayer 1<sup>st</sup> order reflection, hence a multilayer monochromator will reflect the whole undulator harmonic providing “pink beam” operation.

The harmonic selection “efficiency” of the proposed optical layout can be seen in Table 4. Assuming a gap corresponding to the desired 5<sup>th</sup> harmonic centered around 8keV, we calculate the transmission coefficients for all the harmonics by simulating the influence of all the optical elements: total reflection mirror (reflectivity  $R_m$ ), double multilayer (reflectivity  $R$ ) monochromator, and a final exit window (transmission  $T$ ), considered here to be a thin (100  $\mu\text{m}$ ) diamond. The total efficiency of the system is thus  $R^2TR_m$ . All these numbers are calculated in Table 4, showing an estimated efficiency in selecting the desired 5<sup>th</sup> harmonic larger then 50% while all other harmonics are virtually suppressed.

**Table 4** Harmonic acceptance/rejection efficiency of the system consisting in: i) white beam (fixed angle) mirror; ii) multilayer monochromator; iii) 100  $\mu\text{m}$  diamond exit window.

U20 Harmonic #	#1	#3	#5	#7	#9
E [keV]	1.6	4.8	8	11.2	14.4
R - ML reflectivity	0.7	7.5e-3	0.81	3.8e-4	2.7e-4
T (100 $\mu\text{m}$ diamond)	1e-5	0.62	0.90	0.96	0.98
Mirror reflectivity $R_m$	0.94	0.96	0.96	0.13	2.5e-2
Total efficiency $R^2TR_m$	4.61E-06	3.35E-05	0.57	1.80E-08	1.79E-09

It is worthwhile mentioning that at low energy storage rings such as the NSLS-II, it is impossible to achieve efficient pink beam operation with a more simple harmonic selection system that would consist in an absorber working as a high-pass filter in conjunction with the total reflection mirror as a low pass filter. While this is a valid option at high energy machines such as the APS or ESRF where beamlines usually operate using the first harmonic of the undulators, it is much more difficult to select a higher harmonic (e.g., the 3<sup>rd</sup> or the 5<sup>th</sup> at the CHX beamline) and reject the neighboring ones, because they are much closer in energy. A simple calculation like the one shown before shows that in order to achieve a reasonable rejection efficiency of the “undesired” harmonics, the efficiency in accepting the desired one falls to just 1–3%. The coherent flux obtained with such a device would be the same as the one obtained from a “regular” high-resolution Si (111) monochromator, defeating the whole purpose of having a pink beam operation option.

In conclusion, the only practical way of achieving efficient pink beam operation at the CHX beamline is by using a multilayer-based wide bandpass device, and it is our belief that including this option in the baseline layout would enable important early advances in the field.

## 2.5 High Heat Load Optics

A comprehensive set of Finite Element Analysis (FEA) calculations were carried for the DCM using a large variety of finite element models with different cooling schemes. This exercise showed beyond little doubt that water cooling will not be sufficient for this DCM. Essentially this is the case because the small coherent beam that will be utilized at the CHX beamline will create a sharp “thermal bump” on the first crystal (a “standard” Si 111) of the monochromator. Even though the total power deposited by the small beam—e.g., 500  $\mu\text{m}$  (V) x 200  $\mu\text{m}$  (H)—will not exceed 10–12 W, the high thermal gradients would limit the performance of the CHX beamline by creating important distortions of the (first) Si crystal. From this analysis it was concluded that cryogenic cooling will be required in order to solve this problem. The FEA analysis shows that, unsurprisingly, any thermal distortions are almost completely eliminated by the cryogenic cooling.

## 2.6 Beamline Optics and Coherence Preservation

The development of the CHX beamline and other NSLS-II instruments that will focus on applications of coherence will increase the need for X-ray optics with unprecedented figure errors and coherence preservation properties. An important purpose of the NSLS-II project and later operation is to establish a vigorous research program aiming at characterizing the coherence preservation properties of optic elements such as mirrors, multilayers, compound refractive lenses, kinoform lenses, etc. and establishing the guidelines that will allow the improvement of such elements in the near future.

All the mirrors and multilayers will be carefully characterized in the NSLS-II metrology lab (described elsewhere in this conceptual design report) using multiple probes including a Long Trace Profiler, ZYGO stitching interferometer, a Micromap interferometric microscope and an atomic force microscope. Cross-correlation of multiple methods is important in understanding a wide range of spectral frequencies that are critical to the quality of the coherent wavefront. Having a wide range of metrology tools readily available will allow collaborations with selected vendors and suppliers in improving the figure errors by measuring, for instance, the quality of surfaces before and after “corrective” polishing processes.

Ultimately, the best metrology tool is arguably the X-ray beam itself. In a first “at wavelength metrology” experiment performed at beamline ID06-ESRF, we have used an “in-line holography” method (V. Kohn, I. Snigireva, and A. Snigirev, *Phys. Rev. Lett.* 85, 2745, 2000), which consists in measuring the diffraction pattern resulting from the coherent illumination of a well defined object, to evaluate the coherence preservation properties of a synthetic multilayer. As pointed out before, multilayers provide perhaps the only practical way of achieving pink beam operation at NSLS-II. At the same time it is not clear how much they perturb the coherent wavefront. Thus far, the only experience with MLs and coherent beams comes from a few experiments performed at NSLS in the mid 90s (e.g., O.K.C. Tsui S.G.J. Mochrie, *Phys. Rev. E* 57, 2030, 1998). The contrast measured in those experiments was within 30-40% of calculated ones, indicating that the coherence of the beam is preserved, but more investigations, especially new ones using brighter X-ray beams at ESRF and/or APS are clearly needed. In the ID06 experiment we have measured the interference fringes created by a 100  $\mu\text{m}$  diameter Boron fiber directly with a CCD camera or after reflection by a ML structure which was used here as a “sample” (see Figure 11). The ML structure used here was a sequence of 400  $\text{WSi}_2/\text{Si}$  bilayers structure grown in the APS deposition laboratory (R. Conley et al., *Proc. SPIE* 6705, 670505, 2007). The ML parameters and reflectivity are shown in Figure 9. The obvious degradation of the wavefront resulting in the “horizontal stripes” (which can be seen due to the good vertical coherence of beam) is a result of slope errors distributed along the footprint along the ML surface, in this case, a few cm long and 500  $\mu\text{m}$  wide. The substrate used for this test ML structure was a “non-ideal” one in terms of roughness and flatness. Once the NSLS-II deposition facility will become available, we plan to adopt a more “systematic” approach by starting with highly polished, well defined substrates that will be characterized independently before depositing the ML structure.

As shown by Souvrorov et al. (*J. Synchrotron Rad.* 9, 223, 2002) the “distorted” diffraction patterns can be used to retrieve the tangential profile of the additional optical element. Our theoretical approach consists in using a full

wave propagation analysis which takes into account the partial coherent illumination (O. Chubar et al., *Proc. SPIE Int. Opt. Eng.* **4769**, 145, 2002) to retrieve the tangential surface profile of the optical element.

The proposed research program will focus on investigating a multitude of different optic elements by fostering active collaborations with a few vendors and correlating X-ray tests like the one described above with multiple metrology measurements. This will undoubtedly result in systematic and definitive correlations between the metrology data and the quantitative x-ray analysis. We believe this is an important effort that could make a considerable impact in the x-ray community, in which the x-ray optics poses a significant bottleneck to the further advancement of coherence-requiring techniques.

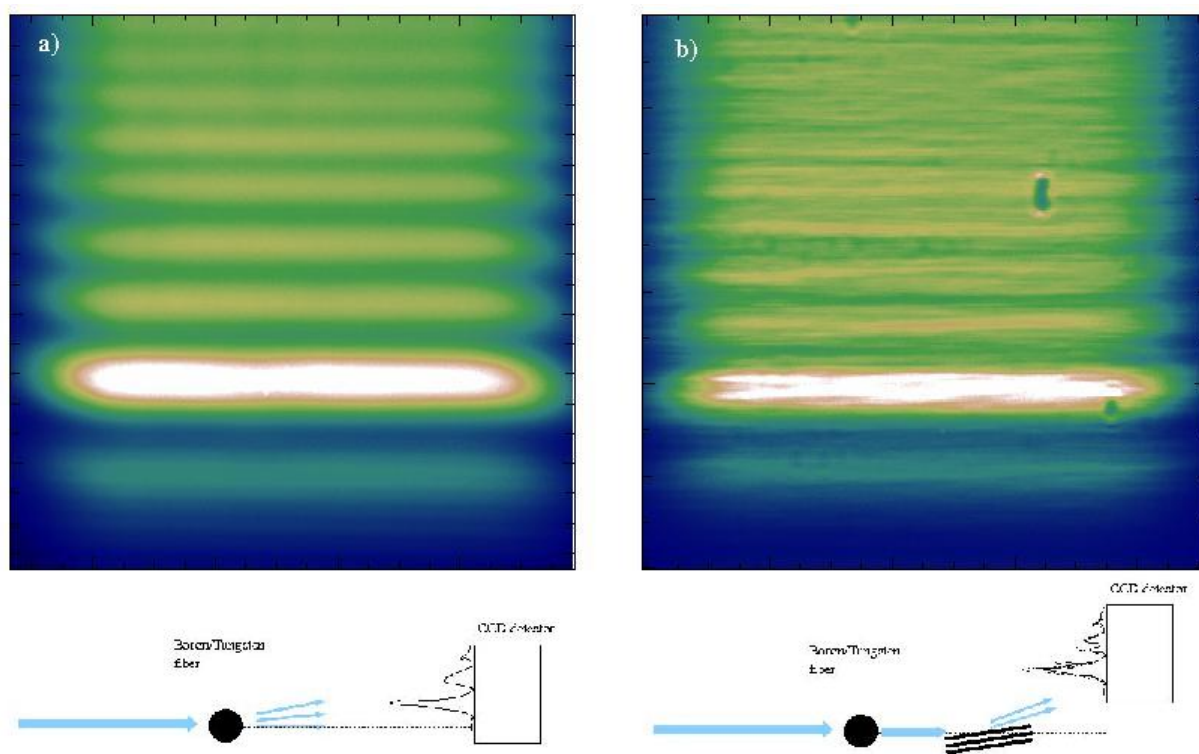


**Figure 11** Interference fringes created by a Boron fiber seen directly on the CCD detector (a) or reflected through a  $\text{WSi}_2/\text{Si}$  ML structure (b). The intensity distribution with the ML was increased by 20% to compensate for losses due to a non-perfect reflectivity and “match” the color scale of the two panels for clarity purposes.

## 2.7 Ray Tracing

An important goal of our optical design was to achieve a large enough separation between the Bremsstrahlung radiation in the forward direction and the pink beam laterally deflected by the total external reflection fixed incidence angle mirror placed upstream. The bremsstrahlung and photon beam ray tracing for beamline optics shown in Appendix 2 demonstrate that the current separation is large enough to allow the design of a tungsten Bremsstrahlung beam stop with an opening for the pink beam about  $\sim 44.8$  mm inboard of the forward direction.

## 2.8 List of Major Components

Table 5 shows the position and approximate size of the beamline components. The space between the main components will be filled with vacuum bellows and pipes of suitable length. The table also shows different sections of the beam line vacuum system.

A CAD drawing of the beam line and the end stations showing general layout of the beam line components is given in Appendix 2.



**Table 5.** List of major components.

Bement	Location (m)	Length (mm)	Description/Notes	Vacuum section
Source	0			
Fixed Front End (FE) aperture	16.21		Can be reduced to ~2 mm	
Lead collimator	16.74			
Beam Position Monitor (BPM) 1	17.43			
BPM 2	19.47			
White Beam Slit, X	20.18		water cooled high heat load	
White Beam Slit, Y	20.78		white beam slits	
Photon shutter	21.17			
Fast Gate Valve	22.1			
Safety Shutter Collimator	22.2			
Dual Safety Shutter	22.98			
	23.36			
Ratchet Wall Collimator	24.02			
Gate Valve 1	25.6			0/1
Differential pump	25.8			1
Gate valve 2 with x-ray window	26			1
Horizontal deflecting mirror	26.5		fixed angle 3.14 mrad, 2 stripes	1
Gate valve 3	26.9			
Bremsstrahlung collimator 1	27.2			1-2
White Beam Slit, X	27.9		"Reduced" version of white beam slits	2
White Beam Slit, Y	28.5		"Reduced" version of white beam slits	
Fluorescent screen	29.1		water cooled	2
Be CRLs	29.31			2
Gate Valve 4	29.65			2-3
Bremsstrahlung collimator	TBD			3
Fluorescent screen, H2O cooled	30.19			3
Double multilayer monochromator	31.3			3
Gate Valve 5	31.65			3-4
Dual crystal monochromator	32.36			4
Gate Valve 6	33.3			4-5
Photon shutter / Bremsstrahlung stop	33.5			5

## 2.9 End Station Instrumentation

A granite table placed just after the wall of the optics hutch will be the first module in the experimental hutch. The table will host a variety of local optics designed for monochromatic or pink beam operation. This will include: focusing optics such as 1D Fresnel Zone Plates or Silicon kinoforms for both vertical and horizontal focusing, local mirror to deflect the beam downwards for GI-SAXS on liquid surfaces, beam defining slits, guard slits, etc. These elements will be kept modular to allow for a certain flexibility, e.g. optimization of distances between slits, etc. All individual elements will be interfaced by vacuum pipes and bellows.

The central piece of the CHX end station (Figure 12) will be a versatile 5-circle diffractometer. A stack of motion controllers offering 3-axis (x, y, z) and 3-circle ( $\theta$ ,  $\phi$ ,  $\chi$ ) positioning will sit on a stable base such as a granite block.

A two-circle ( $\delta, \gamma$ ) detector arm will enable high resolution diffraction experiments in horizontal and vertical scattering geometries. The end station will feature visible on-line microscopy, provided by an on-axis microscope situated just upstream of the sample. In combination with a fluorescent screen, this microscope will also provide excellent beam diagnostic capabilities. WAXS and  $\mu$ -beam SAXS experiments will be performed with the detector held on the diffractometer arm with a sample detector distance up to  $\sim 2$  m and micron size focused beam (both in horizontal and vertical directions).

The SAXS detector and beamstop will be located on a long steel frame upstream of the diffractometer. A selection of working distances for SAXS (e.g. 2m, 5m, 10m, and 15m) will be available through a fast change mechanism for the sectioned flight tube, without the necessity to lift pipes. Detector and beamstop will be equipped with x and z translations for individual alignment respectively to the beam. In the most optimized setting, the setup will allow for a windowless beam path between the beam defining optics and the exit window of the SAXS flightpath.

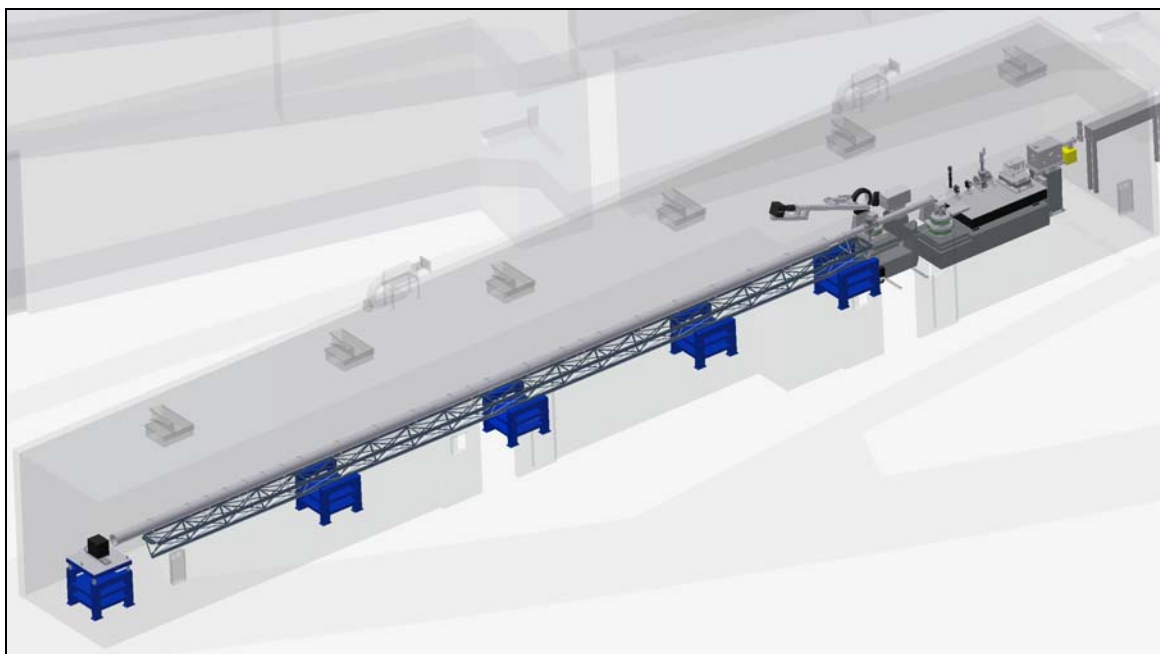


**Figure 12.** Sketch of a proposed end station that will allow SAXS, WAXS, and GI-SAXS experiments.

While offering optimized setups for SAXS and WAXS experiments, the end station will also allow for XPCS studies in SAXS and GISAXS geometries accompanied by (static) WAXS or GIXD measurements. This combination is of particular interest for studies of soft condensed matter systems like e.g. thin organic films or thermotropic gels of self-assembled organic nanotubes. These systems are characterized by an intimate relationship between structure and dynamics, where often the larger scale dynamics is determined by the microstructure.

The vast majority of XPCS experiments will certainly follow the current trend and will require complex sample environments. Flow cells will be used to achieve new functionalities or to avoid beam damage. Shear cells will be used to study driven dynamics in glassy systems, high precision furnaces will be required to study phase ordering processes in materials, Langmuir troughs chambers to study dynamics of ordering phenomena at surfaces, etc. In the standard setup, the diffractometer will host a sample chamber with different insets allowing for temperature control in various temperature ranges between liquid nitrogen temperature and a few hundred degrees.

The CDI setup will be a stand-alone system similar to the one recently developed at the ESRF (ID10C) featuring very high precision motion controllers. This setup could be either hosted on the diffractometer or on the last section of the granite table which supports the local optics. The latter option seems to be in particular favorable for the ptychography and Fresnel approach to CDI, where a very stable positioning of the sample in the incident beam is of utmost importance.

## 3 SPECIAL BEAMLINE REQUIREMENTS

### 3.1 Vacuum

In order to conserve the source brilliance, the beamline will have the possibility of windowless operation. As an option, a selection of “constriction valves” engineered with a window on the blade, will offer the possibility to work with more “relaxed” vacuum requirements during commissioning. In a “maximum brilliance operation” mode, only one final exit window (e.g., Diamond, Be,  $\text{Si}_3\text{N}_4$  ...) placed just before the sample will separate the beamline UHV from the sample environment rough vacuum (or air). A vacuum sensor placed close to the end of the UHV section and a fast valve placed just after the Front End will protect the beamline optics against possible vacuum leaks. A similar system already designed in the Front End will further protect the accelerator vacuum from leaks in the Front End or Beamline Optics

### 3.2 Detectors

A fast 2D photon-counting area detector will be required for the XPCS experiments at NSLS-II. This detector is the most critical element that will enable pursuing the scientific program described in the first part of this document. Unfortunately, at least for the moment, no commercial detector meets our specifications. The two instruments that are the closest in doing that are the Pilatus detector (Dectris) and the Medipix (Medipix Collaboration). Out of the two, the Medipix is the one that was already successfully used in XPCS experiment and enabled results that would have not been possible otherwise (e.g., Chiara Caronna et al. *Phys. Rev. Lett* **100**, 055702, 2008). Unfortunately, the Medipix is not a commercial device and it is not clear if it will become one. More importantly, even if NSLS-II joined the Medipix project (which would perhaps be something advisable) the current maximum full frame readout rate – 1 kHz – is not sufficient for some of the experiments planned at NSLS-II. The Pilatus Detector has the advantage of being commercially available but for the moment is clearly lagging behind in terms of performance (e.g., readout speed, pixel size).

The best alternative for the CHX beamline is a XPCS detector that is currently being developed in a R&D collaboration between the BNL Detector Development Group and Fermi National Laboratory (D.P. Siddons, private communication). The so-called Vertically Integrated Pixel Imaging C... (VIPIC) detector consists in a detector chip bonded to a stack of signal processing “layers” using a “3D integration technology”. A first prototype chip, with the main characteristics described in Table 6, is currently being fabricated and will be connected to a data acquisition controller designed in collaboration with the NSLS-II Controls group. The whole system could be ready for a test experiment as early as the first quarter of 2010.

Other detectors of interest that will need to be available at the CHX beamline include:

- CCD Detector
- A “standard” CCD detector with small pixel size will be used for CDI experiments and/or certain static studies (e.g., SAXS, studies of kinetics via time-resolved SAXS or WAXS, etc.)
- APD array

Fast point-like detectors to be used in conjunction with a hardware correlator will still be required for a certain class of experiment for which the dynamics time scales are typically on the order of  $1\mu\text{s}$  or faster. The clearest example of such class of applications is that of capillary waves at liquid surfaces. The time scales involved in a vast majority of such experiments will likely remain too fast for the next generation of detectors like the “VIPIC” detector. These phenomena will be best studied using a linear array of Avalanche Photon Diode (APD) detectors.

**Table 6.** Main characteristics of the first prototype of the XPCS “VIPIC” detector.

Pixel size	80 $\mu$ m
Number of pixels	64x64
Active area	5120 x 5120 $\mu$ m <sup>2</sup>
Chip size	5.5 x 6.3 mm <sup>2</sup>
Operation:	
Will provide dead timeless readout: each pixels is read sequentially by 2 5-bit counters	
Noise well below 1 photon level ( $\sim 100$ e- vs. $\sim 2200$ e- generated by a 8keV photon)	
Data sparsification will be provided on chip - only the detectors that had a hit will be read.	
Max readout speed 10 $\mu$ s, limited by the estimated max count rate $\sim 0.5$ photons / pixel / 10 $\mu$ s. Readout consists in pixel address, time no. of hits (no energy info).	

### 3.3 Synchrotron Filling Modes

As described before, the NSLS-II CHX beamline will be dedicated to studies of dynamics using XPCS. Obviously any intensity fluctuations coming from other sources—e.g., the filling mode—can perturb the experiment. At ESRF, for instance, the only mode that allows studies of “fast dynamics” on  $\sim 1$   $\mu$ s time scales - is the uniform filling one, in which all 992 buckets around the storage ring are filled, and there are no ion clearing gaps. The proposed NSLS-II baseline mode with has 1/5 of the ring empty as an ion clearing gap, and it is expected that this will not offer “optimal” conditions for this type of measurements (fast XPCS). This will most likely create, pretty much like all other time-structure modes at ESRF do, some very pronounced “spikes” in the correlation functions, precisely around the time scales that need to be measured. However, bunch trains with uniform filling structures will also be possible at NSLS-II. The NSLS-II injector will be able to support virtually any structure. The storage ring itself may operate with a uniform filling (no ion clearing gaps), but the value of the maximum achievable circulating current in this mode is difficult to estimate at this point. Having 100 ns gaps between bunches (uniformly distributed around the ring) would relax the process of ion clearing and enable a high current operation. Such a mode may be appropriate for fast-XPCS, since it should be possible to synchronize the acquisition so that the number of filled buckets within a sampling interval is constant and doesn’t generate any intensity fluctuations.

### 3.4 Data Storage/Handling

With the advent of 2D area detectors with high quantum efficiency and single photon sensitivity, XPCS has become rapidly a technique that produces massive amounts of data. The “typical” XPCS experiment at ESRF or APS easily generates more than 50 GB of data during a single experiment. While this may be considered a “modest” rate compared to high-energy physics experiments, it starts putting a number of logistic problems. First of all, data access rates of 100 MB/s and dedicated optical fiber connection to data storage disks are considered a “minimal requirement”. Data storage capabilities of many TB with automatic backups performed on a regular basis are also required.

While the next generation of XPCS detectors such as the VIPIC system designed by P. Siddons and collaborators will change the current paradigm and use data sparsification in order to increase speed and minimize the amount of unnecessary information that is saved with current systems (e.g. information about pixels that did not receive any photons in a particular time interval), it is reasonable to assume that these developments will not reduce the amount of data that is produced and/or stored, but perhaps only stop or at least reduce the exponential increase in data production that we witnessed over the past few years.

On-line, or quasi on-line data processing starts also being of a critical importance. Not only it starts being difficult for all the users to leave to their home institution with perhaps as much as 100 GB of raw data collected in a one week experiment, but processing this amount of data requires specialized software, training, etc. In many cases

users prefer to leave with semi-processed data – e.g. calculated correlation functions – which they can interpret and further analyze at a later date. For this reason it is mandatory for the CHX beamline to offer high performance and user-friendly software that can be easily used during experiments. This is of fundamental importance as partial results and analysis are actually required in most situations to decide on the optimal experimental strategy.

The strategy in the CHX group is to adopt, further develop, and package in a coherent, comprehensive way software that was designed at other facilities such as the ESRF and APS. In order to minimize problems that are always encountered with property software when new versions are being released and older versions stop being maintained, we will use open source software running on personal computers with linux platforms.

One concrete example is a environment for XPCS data analysis recently developed at ESRF (C. Caronna et. al., *unpublished*). The software is written in Python and offers a user-friendly graphics interface that can be used to calculate equilibrium correlation functions, time-dependent (two-time) correlation functions in non-stationary systems or higher order correlations in systems with dynamical heterogeneities. Such software together with other modules – e.g. for SAXS analysis, data fitting, etc – has to be integrated with the whole instrument, data acquisition, on-line monitoring, software for experimental control, etc.

## 4 FUTURE UPGRADE OPTIONS

### 4.1 Detector Developments

The detector is perhaps one of the most important parts of an instrument such as the CHX beamline. While the current development of the VIPIC detector lead by P. Siddons and collaborators will clearly push very far the current boundaries limiting the performance of detectors for XPCS, it also opens the way for a number of possible improvements: a smaller pixel size, larger detector area, faster readout, more “intelligence” on board (e.g correlation functions, two time correlation functions, on-line “dropletizing” of the detected signal, etc.).

Some of the improvements mentioned above can be more easily achievable with different types of detectors. It is clear, for instance that Avalanche Photon Diodes (APD) detectors will be much faster than other detectors, and an array of APDs will offer unique capabilities for studies of capillary-wave dynamics.

### 4.2 Specialized Sample Environments

Our current efforts are quite naturally centered around developing the best XPCS instrument to date. However, designing the actual experiment and the sample handling instruments and will clearly be equally important. The current trends in the community show beyond any doubt that the stage when a quartz capillary could have been simply “duct taped” in the beam are long gone. The sample environments become increasingly complex, allow for in-situ changes of experimental conditions (e.g. temperature, pressure, atmosphere, electric or magnetic fields, concentration or even composition, etc.). Often there be also an increasing need to perform other measurements in-situ – optical microscopy, rheology, light scattering, etc. or to allow new functionalities with advanced techniques – e.g. time-resolved studies in microfluidic systems (L. Pollack et al., *Phys. Rev. Lett.* **86**, 4962, 2001) or heterodyne/homodyne detection as a means to study the interplay between advective transport and dissipative motion (M. Sutton et al. *in progress*, F. Livet et al., *J. Synchrotron Rad.* **13**, 453, 2006). Last but not least, some of the techniques mentioned above (e.g. microfluidics and heterodyne detection) offer clear advantages in terms of reducing beam damage which is an issue which at NSLS-II will become even more important than already is. From this point of view, it is clear that an instrument like the CHX beamline (or any other beamline at NSLS-II) will require continuous developments of new sample environments or improvements of existing ones.

### 4.3 Beamline Optics and Figure Control

The development of improved optics with better coherence preservation properties will continue to be a major preoccupation in the CHX group throughout the later operation of the beamline. The ultimate goal is to achieve an

efficiency as close as possible to 1 in using the entire coherent flux available from the NSLS-II source by improving the surface finishing of the optical elements, reducing the heat load, finding technical solutions to use new materials (e.g. better quality diamond than is available today). The use of focusing K-B mirrors for applications using coherent beams will also be investigated.

#### Upgraded Insertion Devices

Simulations of possibly upgraded in-vacuum undulator sources are shown (courtesy of Oleg Chubar) in Figure 13. The calculations assumed an electron current in the ring of 500 mA, a “day one” horizontal emittance of 0.9 nm (the fully damped value is 0.5 nm) and energy spread of  $8.9 \times 10^{-4}$ . The simulation shows the spectral brightness of a longer undulator, assuming the technology will allow an increased magnetic field to compensate for an increased vertical gap (the maximum K value is the same as for the current U20 IVU).

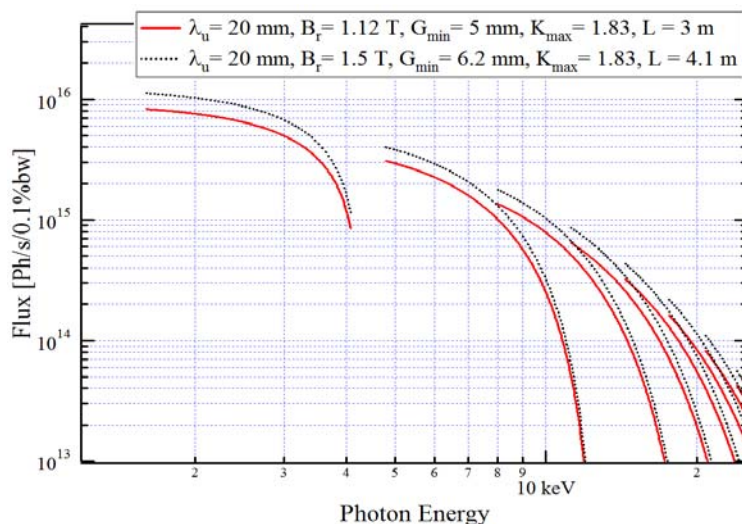


**Figure 13.** Spectral brightness for the odd harmonics with an (hypothetical) upgraded longer undulator with a higher magnetic field. (courtesy of Oleg Chubar)



## APPENDIX 1 SCHEDULE

### Construction of CHX beamline

Oct. 2009	Complete Conceptual Design Report
Sept. 2010	Complete Preliminary Design Report
Dec. 2010	Technical Design – Approval of Long Lead Term Procurement
Jan. 2011	Start Lead Time Procurements (monochromators, CRL, enclosures,...)
Apr. 2011	Complete Final Design of Beamline Major Components
Feb. 2012	Complete Final Design Report
Feb. 2012	Approval of Start of Beamline Construction - Beneficial Occupancy of Experimental Floor
Feb. 2012	Start Installation
May 2012	Start Sub-System Testing
May 2012	Start Other Procurement
Jan 2013	Complete Long Lead Time Procurements
Aug 2013	End Procurement
Aug 2013	Start Integrated Testing
Jan 2014	Complete Installation
Feb 2014	Complete Sub-System Testing
May 2014	Complete Integrated Testing – Beamline available for Commissioning
June 2015	<b>CD-4</b> , Approve Start of Operations

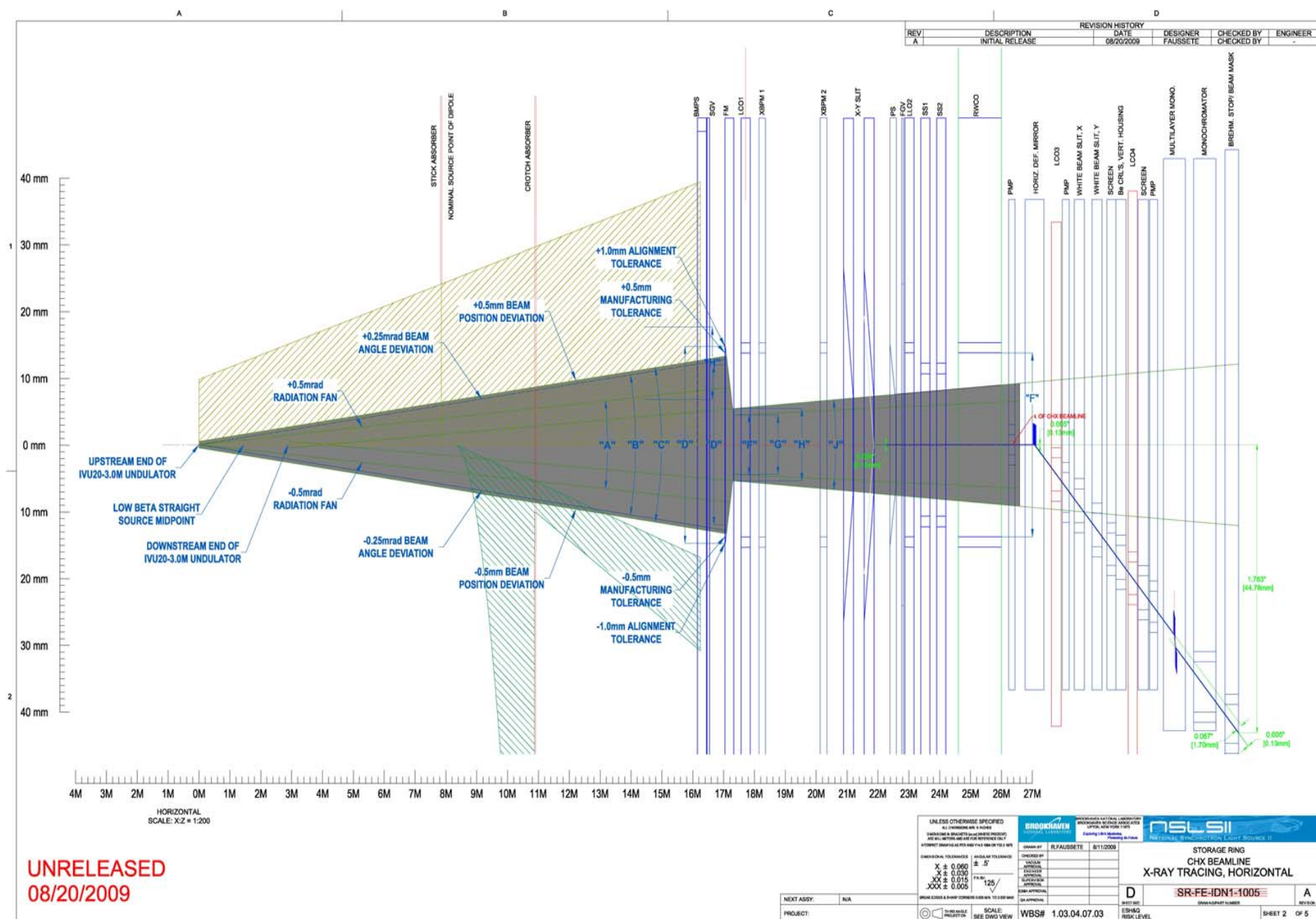
*Intentionally blank.*

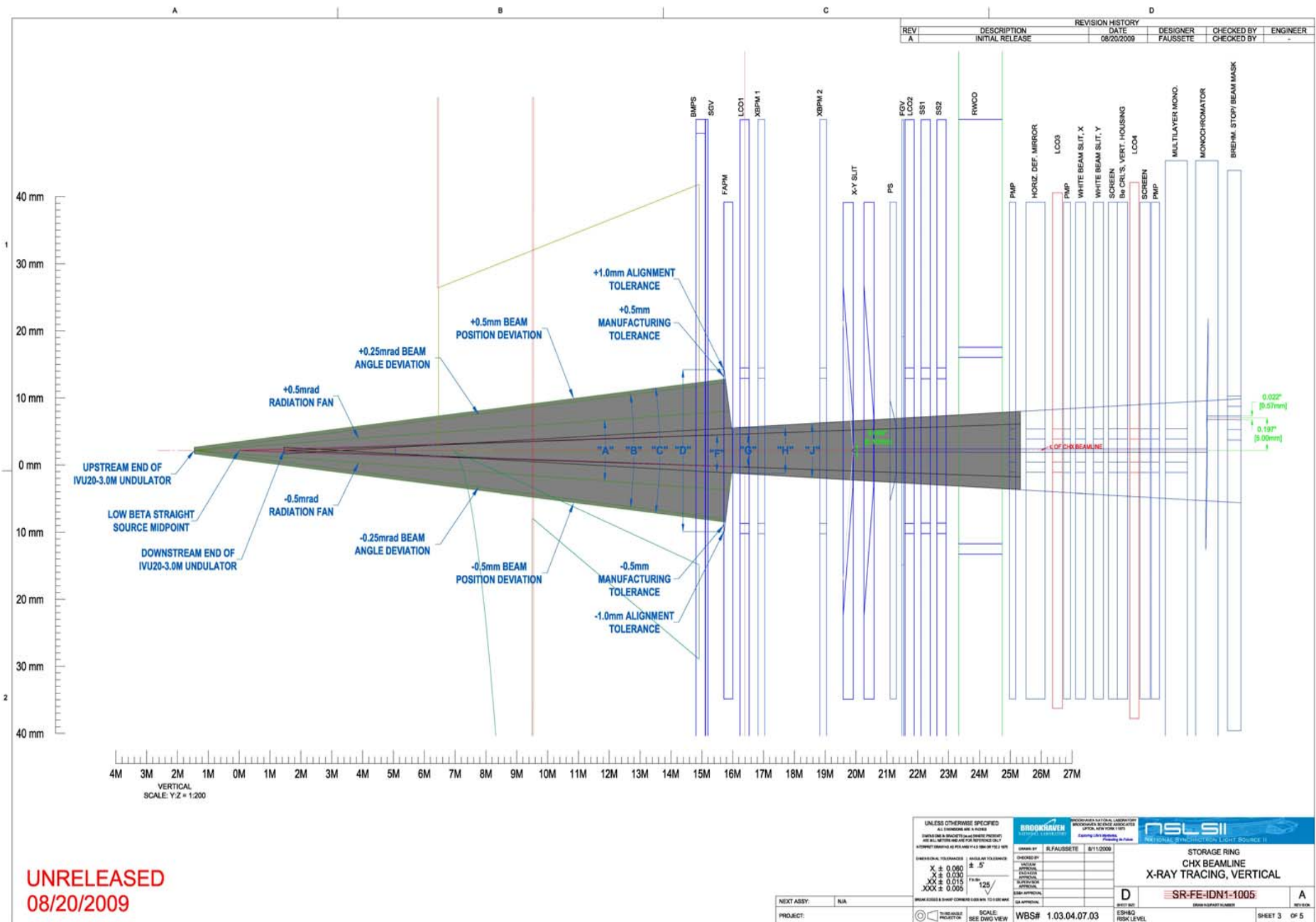


## **APPENDIX 2      REFERENCE DRAWINGS**

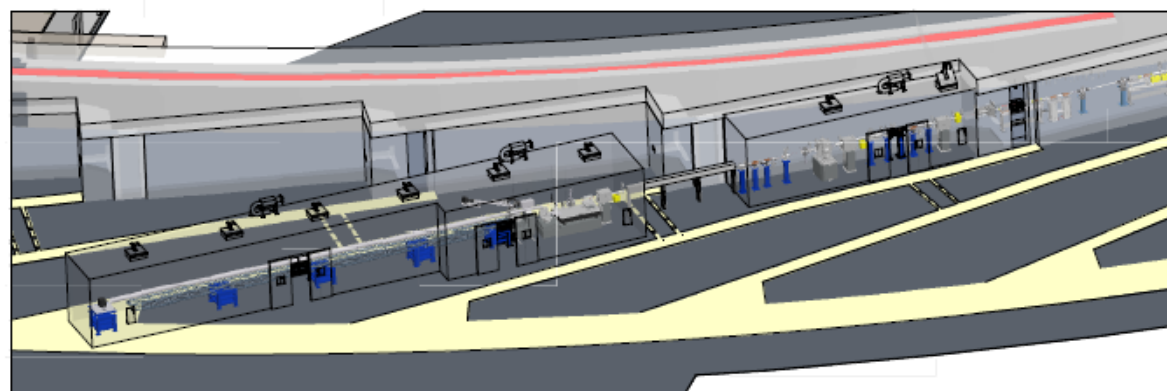
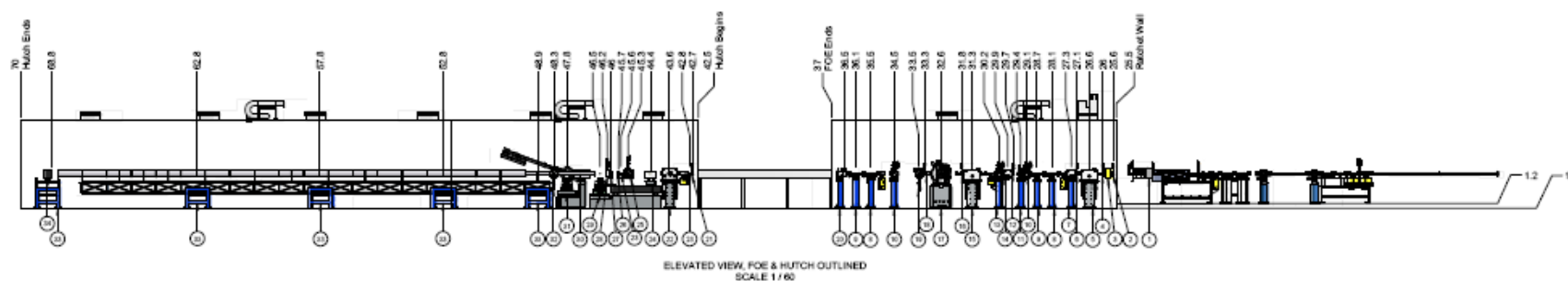
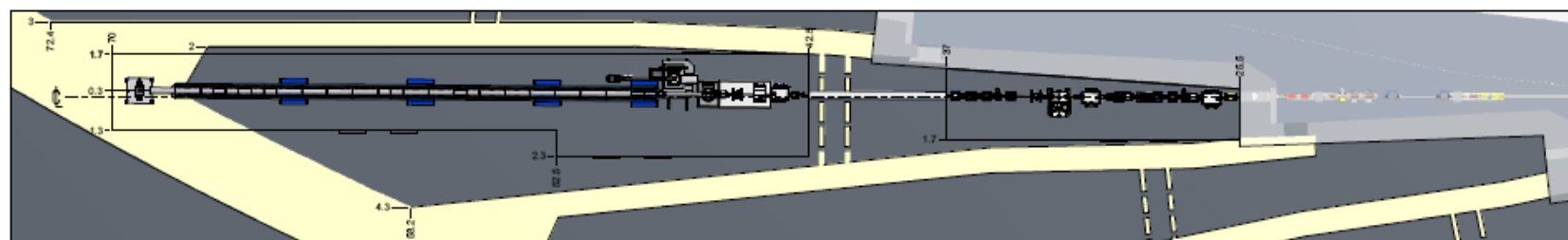












PRELIMINARY  
9/25/09

Dimensions are in meters from source.

PARTS LIST				
ITEM	QTY	DESCRIPTION	PART NUMBER	VENDOR
1	1	Short Straight Front End CHA	SE-FE-DNT-1200	
2	1	Gate Valve 1		
3	1	Differential Pump		
4	1	Gate Valve 2 with X-Ray Window		
5	1	Horizontal Deflecting Mirror		
6	1	Gate Valve 3		
7	1	Bremsstrahlung Collimator 1		
8	2	White Beam SLI, X		
9	2	White Beam SLI, Y		
10	2	Fluorescent Screen, H2O Coated		
11	1	for CR's, Vertical Focusing		
12	1	Gate Valve 4		
13	1	Fluorescent Screen Beam Monitor		
14	1	Bremsstrahlung Collimator 2		
15	1	Multi-layer Monochromator		
16	1	Gate Valve 5		
17	1	Monochromator		
18	1	Gate Valve 6		
19	1	Pink Beam Stop		
20	1	Mask, Photon Shutter & Beam Stop		
21	1	Gate Valve 7		
22	1	VF2P, HP2P or Kinofone, Hor. Mirror		
23	1	Diamond (or Be/Polymer) Exit Window		
24	1	KB Mirror System		
25	1	Pink Shutter		
26	1	Beam Defining Aperture, Precision Silt		
27	1	Pink Beam Aperture, Precision Silt		
28	1	Microscope Assembly		
29	1	SAXS Gonimeter		
30	1	SAXS Right Path		
31	1	SAXS Shutter		
32	1	APD & Beamstop		
33	5	Detector Support		
34	1	Detector		
35	1	NSLS-II Building Assembly	BP-CF-1001	